NASA Technical Memorandum 84232

Static Investigation of the Circulation-Control-Wing/Upper-Surface-Blowing Concept Applied to the Quiet Short-Haul Research Aircraft

J. C. Eppel, M. D. Shovlin, Dean N. Jaynes,
R. J. Englar, and J. H. Nichols, Jr.

(NASA-TM-84232) STATIC INVESTIGATION OF THE CIRCULATION CONTROL WING/UPPER SURFACE BLOWING CONCEPT APPLIED TO THE QUIET SHORT HAUL RESEARCH AIRCRAFT (NASA) 49 p
HC A03/MF A01 CSCL 01C G3/05
N82-32343
Unclas
28899

July 1982

NASA
National Aeronautics and
Space Administration

NASA Technical Memorandum 84232

Static Investigation of the Circulation-Control-Wing/Upper-Surface-Blowing Concept Applied to the Quiet Short-Haul Research Aircraft

J. C. Eppel
M. D. Shovlin
D. N. Jaynes, Ames Research Center, Moffett Field, California
R. J. Englar
J. H. Nichols, Jr., David Taylor Naval Ship Research and Development Center,
Bethesda, Maryland

NASA
National Aeronautics and
Space Administration

Ames Research Center
Moffett Field, California 94035

STATIC INVESTIGATION OF THE CIRCULATION-CONTROL-WING/UPPER-SURFACE-BLOWING CONCEPT APPLIED TO THE QUIET SHORT-HAUL RESEARCH AIRCRAFT

J. C. Eppel, M. D. Shovlin, D. N. Jaynes, R. J. Englar,* and J. H. Nichols, Jr.*

Ames Research Center

SUMMARY

Full-scale static investigations have been conducted on the Quiet Short-Haul Research Aircraft (QSRA) to determine the thrust-deflecting capabilities of the circulation-control-wing/upper-surface-blowing (CCW/USB) concept. This scheme, which combines favorable characteristics of both the A-6/CCW and QSRA, employs the flow-entrainment properties of CCW to pneumatically deflect engine thrust in lieu of the mechanical USB-flap system. Results show that the no-moving-parts blown system produced static thrust deflections in the range of 40°-97° (depending on thrust level) with a CCW pressure of 2.089 × 10^5 Pa (30.3 psig). In addition, the ability to vary horizontal forces from thrust to drag while maintaining a constant vertical (or lift) value was demonstrated by varying the blowing pressure. The versatility of the CCW/USB system, if applied to a STOL aircraft, was confirmed, where rapid conversion from a high-drag approach mode to a thrust-recovering waveoff or takeoff configuration could be achieved by nearly instantaneous blowing-pressure variation.

INTRODUCTION

Research in powered-lift aerodynamics to provide STOL characteristics for both military and commercial aircraft has led recently to the development of both the NASA Quiet Short-Haul Research Aircraft (QSRA), built by the Boeing Commercial Airplane Co[illegible]ny, and the Navy/Grumman A-6/Circulation Control Wing (CCW) flight demonstrator aircraft (figs. 1 and 2). In a recent concept developed by the David Taylor Naval Ship Research and Development Center (DTNSRDC), the flow-entraining properties of the CCW trailing edge are utilized to deflect engine thrust in a manner similar to that in the upper-surface-blowing (USB) concept used in the QSRA and YC-14 aircraft.

The concept benefits from powered-lift characteristics similar to those of the QSRA and YC-14 aircraft, but obtains those characteristics pneumatically instead of mechanically. The CCW/USB concept is shown schematically in figure 3 and is shown in a twin-engine STOL aircraft configuration proposed by DTNSRDC in Figure 4. On the proposed aircraft, both the outboard CCW lift-augmenting wing section and the inboard CCW/USB thrust-deflecting section are composed of small, circular, no-moving-parts trailing edges; the mechanical flaps otherwise used on the QSRA and YC-14 are completely eliminated. Both inboard and outboard systems have been investigated statically and dynamically in model scale (refs. 1-4), and CCW alone has been

---

*Aircraft Division, David Taylor Naval Ship Research and Development Center, Bethesda, Maryland.

flight-verified (refs. 5 and 6); however, full-scale operation of the CCW/USB configuration in the mixed flow exhaust of a turbofan engine had not been attempted.

The QSRA is a NASA flight research facility used to develop propulsive-lift concepts. Hence, a joint NASA/Navy static test was undertaken, with a representative CCW/USB configuration installed behind one engine of the QSRA aircraft, which was undergoing propulsion-system/airframe interaction testing on static thrust stands at Ames Research Center. The present investigation was intended to confirm full-scale static-thrust deflection produced by CCW/USB, compare that thrust-turning to model-scale results, and identify any problems produced by the mixed-flow exhaust of a turbofan engine.

Contributions by Patricia Nerio, design of the CCW trailing edge hardware; Henry G. Montoya, fabrication of the CCW trailing edge hardware; Dalton L. Mountz, aircraft operations; Michael Moniuszko, instrumentation; and Michio Aoyagi, in support of data system development, are gratefully acknowledged.

SYMBOLS

A_j	CCW slot exit area, m^2 ($in.^2$)
A_{noz}	engine nozzle exhaust area
a_j	speed of sound in CCW slot exit, m/sec (ft/sec)
C_μ	$\frac{\dot{m} V_j}{A_j}$, $\frac{\text{lbs}}{\text{in.}^2}$
F	calculated or measured force, N (lb)
G_{fuel}	fuel volume used, m^3 (gal)
g	acceleration due to gravity, m/sec^2 (ft/sec^2)
h_{nom}	nominal unpressurized CCW slot height
h_j	CCW slot height, m (in.); actual pressurized CCW slot height
I	initial force or loading measured at load pad, N (lb)
K_a, K_b	balance temperature sensitivities, 1/°C (1/°F)
K_x, K_z	first-order balance sensitivities, 1/N (1/lb)
$K_{x,z}$, $K_{z,x}$	second-order linear balance sensitivities, N/N (lb/lb)
$K_{x,xz}$, $K_{z,xz}$	second-order nonlinear balance sensitivities, 1/N (1/lb)
L	measured load or force at each load pad, N (lb)
M_{USB}	engine exhaust mach number near CCW slot
M_j	CCW slot Mach number

$\dot{m}$	$\dot{w}/g$ slot mass flow rate kg/sec (slugs/sec)
mv	strain-gage balance output, V
N_1	fan speed
P	pressure, N/m^2 ($lb/in.^2$)
P_{ref}	standard day atmospheric pressure, $lb/in.^2$
R	universal gas constant; $R_{air} = 53.3 \frac{ft\text{-}lb}{lb°R}$
T	temperature, °C (°F)
T_{ref}	standard day atmospheric temperature, degrees
t_c	calibration temperature of flexure beam, °C (°F)
t_1	balance temperature at static measurement, °C (°F)
$T_{installed}$	installed engine thrust, including flap, nozzle, nacelle, and vortex generator losses
$T_{resultant}$	resolved engine thrust after turning
t_2	balance temperature during load measurement, °C (°F)
V	velocity, m/sec (ft/sec)
v	balance excitation voltage, V
W_{fuel}	weight of fuel, N (lb)
δ_{USB}	USB flap deflection angle
$\dot{w}$	slot weight flow rate: $(\dot{m})(g)$; $\left(\frac{lbs}{sec}\right)$
θ_R	resultant force angle (see fig. 17), rad (deg)
θ_w	wind angle to aircraft body axis, rad (deg)
ρ_{fuel}	fuel density, kg/m^3 (lb/gal)
γ	$\frac{c_p}{c_v}$; ratio of specific heats. Air at std. cond., $\gamma = 1.4$

Subscripts:

a	air
d	duct; CCW plenum; total pressure or temperature
i	1,2,3; station location (see fig. 17)
j	jet

ORIGINAL PAGE IS
OF POOR QUALITY

R	resultant
W	wind
X	horizontal
Z	vertical
∞	free stream, ambient

AIRPLANE DESCRIPTION

The QSRA is shown making a carrier approach in figure 1, and the aircraft's general configuration is shown in figure 5. The fuselage is that of a deHavilland C-8A Buffalo with structural reinforcement in the aft section and new fairings at the wing-body intersection. The C-8A empennage was used without structural or aerodynamic modification, but the landing gear was modified to increase the sink rate capability of the aircraft.

The QSRA wing, designed and fabricated by Boeing, has a wingspan of 22.4 m (73.5 ft), a wing area of 55.74 m^2 (600 ft^2), and quarter chord sweep of 15°. The center section of the wing is sealed to form two integral fuel cells which contain a total of 4535.9 kg (10,000 lb) of Jet A-1 (JP-5) fuel. The fixed leading-edge flaps are slotted in order to provide boundary-layer control aerodynamically. The trailing edge on either side of the centerline consists of two USB flaps, a double-slotted flap, and a drooped, blown aileron. (Additional aircraft descriptive information is contained in ref. 7).

PROPULSION SYSTEM

The QSRA propulsion system consists of four AVCO-Lycoming YF-102 (QSRA) engines mounted in above-the-wing nacelles. These prototype engines, acquired from the USAF A-9A program, are geared fan jets with a bypass ratio of six to one; they are similar to the AVCO-Lycoming ALF-502L commercial engine or the General Electric TF-34 engine.

The engine weighs 5,412 N (1,215 lb), has a basic diameter of 1.077 m (42.4 in.), and an overall length of 1.62 m (63.8 in.), including the fan spinner; the fan has a diameter of 1.024 m (40.3 in.). Although the rated thrust of the engine is 33,361 N (7,500 lb), the standard-day value of installed thrust is about 27,801 N (6,250 lb). Detailed information on the engine performance characteristics and the propulsion system design is given in reference 8.

QSRA PROPULSIVE-LIFT SYSTEM

The external nacelle (fig. 6) of the QSRA is composed of two main assemblies. The structural cowl and nozzle assembly is attached to the wing front spar and the engine build-up assembly is mounted to this structure. An inlet is attached to the

ORIGINAL PAGE IS
OF POOR QUALITY

engine as shown in figure 6; it serves as both the inlet and outer nacelle. Fire protection is provided behind the nacelle by an external heat shield attached to the upper surface of the wing, together with the use of heat-resistant materials in the wing flaps and trailing edge.

Nozzle Design

The exhaust system is a confluent-flow design with both primary and fan streams discharging through a common D-shaped exit nozzle having an aspect ratio of 3.5. As indicated in figure 6, the core exhaust diffuses as it passes through the primary nozzle and then mixes with the surrounding fan stream before exiting through the D-shaped USB nozzle. The core nozzle is canted upward 9.4° relative to the engine centerline to minimize heat effects on the wing.

The flow areas in the fan duct and core-nozzle exit plan (mixing plane) were sized to provide adequate performance without affecting engine stability. The main control on stability margins and engine-match, however, is provided by the final exit area of the D-nozzle. The exit is designed to spread the exhaust into a thin sheet, which is then turned, in accordance with the Coanda effect, over the USB flaps, thus providing propulsive lift. The efficiency of the jet sheet in providing this propulsive lift is highly dependent on the design and shape of the D-nozzle exit. For the QSRA, this flow spreading is enhanced, especially with one engine inoperative, by a cutout that opens toward the adjacent nacelle.

Jet Spreading

Figure 7 shows the cutout in the right inboard engine nozzle. In normal circumstances, this cutout improves wing and flow-turning efficiency by inducing a spanwise component of flow and spreading the thin jet sheet over some portion of the adjacent USB flap during engine-out operation. For this test, however, this spanwise component of flow induced the jet sheet to extend beyond the physical boundaries of the CCW trailing edge and thereby slightly decreased its turning potential.

Jet Mixing and Rotation

Two other characteristics of the QSRA powered-lift system may also have had an adverse effect on the CCW trailing edge performance; they are the vortex generators and exhaust vanes.

Vortex generators – There are two rows of vortex generators located behind each engine (fig. 7). The forward row is designed to improve the mixing and turning of the primary flow and to energize the boundary layer. The aft row was developed to maximize lift at low angles of attack with an engine inoperative during flight. Although the effect of these vortex generators on the CCW trailing edge is not known, they do increase flow turbulence, especially in the USB-jet boundary layer. This increased turbulence may induce a higher than normal mixing between the USB jet and CCW-jet sheet, thereby reducing its turning potential.

Exhaust vanes – Another characteristic of this propulsion system is that the engine was designed for the A-9A application and has a set of turning vanes in the primary nozzle that maximize thrust at high power settings but introduce a rotational component in the primary flow at low power settings. This leads to significant rotational velocity components in the USB jet at low to intermediate power settings. These rotational flow components are known to affect spreading and to cause the jet to move in a spanwise direction when the jet is deflected (ref. 8). The net effect of this flow movement is to reduce the effective turning angle of the USB flaps; hence, it would also decrease the turning potential of the CCW trailing edge at low to intermediate power settings. This effect is partially offset by the vortex generators.

CCW TRAILING EDGE DESIGN

This investigation was intended primarily as a full-scale static proof of concept. Therefore, the test configuration was developed as a simple bolt-on configuration to be installed behind one inboard QSRA engine only. Since no flight testing was intended, the configuration was not designed to be airworthy, and the air supply to the CCW trailing edge was provided from external ground air-start carts instead of from engine bleed. The test configuration (fig. 8) is based on CCW parameters supplied by DTNSRDC and found effective in past development. The rather large-diameter circular pipe was based on the trailing edge tested in reference 3, and was installed to assure adequate CCW jet attachment and engine thrust turning. Smaller diameters are being investigated in model-scale. Ames Research Center was responsible for configuration design, construction and installation of the CCW device, test setup, instrumentation, and data reduction.

Mechanical Design

Aluminum was chosen as the design material because of its availability and light weight. The CCW device could not be mounted directly at the trailing edge of the USB flap because the flap bracket fairings protruded aft of the flap and slightly above it; this necessitated the long plate leading up to the nozzle, as shown in figure 9. The CCW was to be mounted on a series of existing brackets located on the under surface of the flap, which had been used for other test hardware; hence, the requirement for light weight. Further calculations showed that the air-hose connections (fig. 10) and the lift that would be generated on the CCW trailing edge with high USB thrust levels exceeded the strength of these existing brackets. As a result, the flap support was redesigned so that the loads were transmitted directly from the CCW trailing edge to the main landing gear by a support strut (fig. 11).

<u>CCW trailing edge</u> — The end view of the CCW trailing edge (fig. 9) shows its major components: (1) the 0.254-m (10-in.) dia. tube, which provided both the turning surface and the air supply inlet; (2) the welded plenum chamber; (3) the plate, which is also the adjustable nozzle; and (4) the air-supply-cart hose connections.

<u>Turning surface</u> — A standard 0.245-m (10-in.) dia. tube was chosen in order to provide the required CCW radius with a high degree of precision. As shown in figure 9, two air-supply-cart hose fittings were installed on the lower surface approximately 3.14 rad (180°) from the adjustable nozzle. A series of holes between the pipe and plenum assure even distribution of air with low Mach Number (less than 0.2) even at the maximum air-flow rate of 1.82 kg/sec (4 lb/sec).

<u>Instrumentation</u> — Static-pressure and temperature instrumentation was installed in the plenum chamber at the center of the plenum between the supply pipes and at the outboard end of the plenum. This instrumentation was so installed that the pressure

and temperature measurements were made at the level of the row of supply holes into the plenum and thus could give an indication of the uniformity of the plenum air flow.

Problem Areas

Aluminum was chosen for strength based on some preliminary estimates of the air-supply temperature. During the initial proof test it was found that the temperature of the air in the air-supply ground carts was running about 30°C to 40°C higher than anticipated; the result was a significant reduction in material strength and structural life. A second problem area involved the effect of this design on the CCW jet's static turning efficiency. It was noted that air leaks at the plenum edge, combined with edge effects, resulted in reduced turning over approximately the 0.05- to 0.07-m (2-3-in.) length from each end. In addition, there was a reduction in turning in the vicinity of the air-start ground-cart hose inlets. Both of these effects were noted qualitatively during the proof tests, but quantitative measurements of loss of static turning could not be made. Although the influence of these effects on the installed CCW-USB turning cannot be determined, it may be assumed that turning would be slightly less than predicted from previous tests.

GROUND TEST

Aircraft Force Measurements

The lift and thrust forces and, hence, turning angle, acting on the QSRA were determined by summing the axial and normal forces acting on the landing gear. These axial and normal forces were measured at each gear station by a load pad, using a calibrated strain-gage flexure beam. These load pads, originally developed by Boeing for QSRA ground tests, are bolted to steel anchor plates installed on one of the aircraft run-up areas at the Ames Research Center V/STOL Test Site. The main landing gear and nose gear load pads are shown in figure 12, and the aircraft is shown mounted on the load pads in figure 13. The airplane wheels are firmly clamped to a plate mounted on top of the load pads, and the airplane is leveled with respect to the horizontal. Plywood shields are located behind the main gear pads to prevent hot gas impinging on the load pads during engine operation wit high flow turning angles. The load pads are electrically heated to minimize strain-gage temperature fluctuations and to keep moisture off the flexure beam and the strain-gage terminal strips. The load-pad temperatures and strain-gage excitation voltages were manually recorded before and after each run and the strain-gage outputs were channeled into the aircraft's flight data system and recorded continuously. The strain-gage bridges are excited by the regulated power supplies built into the aircraft's data system.

Aircraft Data System

The QSRA is equipped with a high-speed data system composed of transducers, signal conditioning equipment, a telemetry transmitter, and a tape recorder. This system makes measurements, telemeters data in real time to a ground data facility, and records significant airplane and ground instrumentation parameters for post-test analysis.

Data from the transducers are transmitted to the analog and digital network panels, which provide the necessary signal conditioning. The conditioned data then pass to the remote multiplexer-digitizer unit (RMDU), which adjusts the gains to a programmed level, provides analog to digital conversion, and encodes the data in a pulse-code modulated serial bit stream. The data from the RMDU are recorded on a standard 14-track, airborne, magnetic tape recorder; they are also telemetered via L-band transmission to a ground station for real-time data monitoring. The aircraft data system contains a time-code generator, which furnishes correlation for the data. Separate, precision low-voltage power supplies located in the aircraft's analog network panels furnish transducer excitation power where required. A more detailed description of system elements is given in reference 7.

Meteorological Measurements

The aircraft is equipped with instrumentation that accurately measures atmospheric conditions in flight; however, most of these sensors are of limited use during ground testing. In order to have an accurate assessment of the wind speed and direction, air temperature, humidity, and barometric pressure, a Met One weather station was installed on the test site. This station (fig. 14) was located several hundred feet from the aircraft at about wing level. This location was chosen so that the atmospheric readings would be representative of those at the aircraft but would not be influenced by it or the ground-support equipment. The meteorological data are converted to both direct readout and to analog signals by the Met One weather station. The direct readout was used as an aid by test personnel at the site, and the analog signals were channeled into the aircraft data system, giving a continuous record of atmospheric conditions during the test.

Test Procedures

The data are telemetered to a ground station for real-time processing and are also recorded for post-test analysis. The test is directed from the ground station with radio communication links between the test site, aircraft, and the ground station.

Test plan — The general plan consisted of advancing the left inboard engine power settings (fan speed) in even 5% increments from ground idle to maximum power and then decreasing the settings in the same manner. Each setting was held for 30 sec before proceeding to the next condition. A list of the individual test conditions is given in table I. Static measurements were made before and after each data run in order to verify data system operation and to provide the loads-history required for analysis.

Because the CCW trailing edge was installed before the beginning of the test, the first run was made with the CCW nozzle gap set at 0.102 cm (0.040 in.) with no air flow through the nozzle. This test condition set a baseline thrust and turning-angle measurement versus fan speed and also allowed the CCW device to heat gradually without being under pressure. For the next run the engine was shut down and the CCW slot was gapped to the nominal 0.102 cm (0.040 in.) size. Figure 15 shows two technicians adjusting the nozzle gap. The CCW plenum was then operated at maximum pressure and temperature until all pressures and temperatures in the CCW trailing edge were stable.

Based on the results of this run, it was decided that testing would continue with the nominal gap. (When hot, the CCW nozzle gap was about 10% greater than at the cold settings, and it increased approximately 70% to 75% when hot and under

30.33×10^4 Pa (44 psia) pressure to about 0.170 cm (0.067 in.). The next two runs were made, respectively, with two air carts and with one air cart providing air to the CCW trailing edge while the engine was operating. The next two runs were made with the CCW trailing edge nozzle gapped to 0.052 cm (0.020 in.) cold; again the runs were made first with two air carts and then with one air cart providing air to the slot.

Operational problems – In addition to supplying air for the CCW plenum, the air-start carts also supply electrical power to the aircraft. During the test there were several power interruptions to the aircraft electrical system that runs the data system and powers the sensors. These interruptions were caused by the aircraft's frequency protection devices activating in response to the speed fluctuations in the air-start cart's power unit during pressurization of the CCW. Although these power interruptions were not serious from an operations standpoint, they did reset the fuel totalizers to zero and thus affected the real-time lift calculations.

Because of the uncertainty that these power interruptions introduced into the real-time data and because the slot height had not been measured with the CCW device both hot and under pressure, the test was repeated the next day with the larger gap setting. Toward the end of the test series the CCW pressure began dropping; on inspection, it was noted that the adjusting screws were working loose, which caused the nozzle slot to grow non-uniformly. After repairing the nozzle upper plate and adjusting screws, the test was run again; the pressure then held steady during the entire test series.

Baseline measurement – Upon completion of the CCW test series the CCW assembly was removed and the USB flap restored to its original configuration. Then an additional test series was run following the identical procedure in the CCW test plan in order to provide a baseline thrust and turning-angle measurement for the USB flap.

Real-time data processing – The data were telemetered to the ground station for real-time data processing. The telemetered data stream was decoded, converted to engineering units, and each measured parameter was sampled five times a second. Because of equipment limitations, hard-copy updates of the entire parameter list were only obtained every 4 sec. Real-time processing was used to provide a check of the results to determine the validity of selected parameters that were displayed continuously on strip charts and also on alpha-numeric television displays. These parameters included the CCW temperature and pressure; engine speeds, temperatures and pressures; atmospheric conditions; load pad axial and normal forces at each landing gear location; and calculated values of the net lift, thrust, flow-turning angle, and CCW slot jet velocity.

The load-pad force calculations were simplified for real-time processing by only accounting for the first-order linear components from the balances (see Analysis section). The net thrust was calculated by summing the axial forces from the landing gear load pads. The net lift was obtained in a similar manner from the sum of the load pad normal forces; however, it had to be corrected for the weight of the airplane. The weight of the airplane was calculated by subtracting the weight of fuel used during testing from the initial airplane weight, as recorded by the load pads. This fuel weight was obtained from the aircraft's fuel totalizers, which record the amount of fuel used by each engine. Finally, the resultant thrust was calculated by taking the vector sum of the lift and axial forces; the turning angle was the angle between the resultant and the horizontal forces.

ORIGINAL PAGE IS
OF POOR QUALITY

ANALYSIS

External Force Measurements

The axial and normal forces at each landing gear location were measured with a calibrated flexure beam, instrumented with a set of orthogonal strain-gage bridges. The primary effects on these bridge outputs were the level of force, axial or normal, in the direction the bridge was designed to measure, and the value of input excitation voltage to the bridge. Besides these primary effects, several secondary effects also had to be considered to accurately calculate the input loads from the strain-gage outputs. The two most important of these effects were the temperature variation of the flexure beam during the test versus its calibration temperature, and the interaction of axial and normal force through the flexure beam.

Calculation procedure — The procedure for determining the load-pad forces consisted of two operations: calculating the initial loads under static conditions and using the outputs of the strain-gage bridges in conjunction with the static loads to determine the actual test axial and normal forces. Since the equations for each load pad are similar (except for different constants), this discussion will only show the procedure for determining the loads from one load pad. Because the load equations contain interaction terms, the normal procedure is to start with a value based on no interactions, and then to iterate the equations, using the previous solution in each successive iteration. This procedure is continued until the difference between iterations is less than 0.005%.

Static load calculation — The static loads are calculated in the following manner.

The initial loads iteration:

$$I_X = \frac{mv_X}{v_X K_x [1 + K_a (t_1 - t_c)]}$$

and

$$I_Z = \frac{mv_Z}{v_Z K_z [1 + K_a (t_1 - t_c)]}$$

Subsequent loads iterations:

$$I_X = \frac{mv_X}{v_X K_x [1 + K_a (t_1 - t_c)]} - \{K_{x,z}\, I_Z + [1 + K_b (t_1 - t_c)]\, K_{x,xz}\, I_X\, I_Z\}$$

and

$$I_Z = \frac{mv_Z}{v_Z K_z [1 + K_a (t_1 - t_c)]} - \{K_{z,x}\, I_X + [1 + K_b (t_1 - t_c)]\, K_{z,xz}\, I_X\, I_Z\}$$

The initial or static loads are calculated for each data point over a 30-sec period and then an average is taken for the entire sample of approximately 150 points. These initial or static loads along with their average load-pad temperatures and excitation voltages are recorded for later use in determining the test loads and also in checking the load pads' strain-gage stability.

<u>Test loads calculation</u> — Once the initial loads have been determined, the balance loads during a test condition are completed in the following manner.

The first iterations:

$$L_X = \frac{\Delta mv_X - B_X}{v_X K_x [1 + K_a(t_2 - t_c)]}$$

and

$$L_Z = \frac{\Delta mv_Z - B_Z}{v_Z K_z [1 + K_a(t_2 - t_c)]}$$

where

$$B_X = v_X K_x [K_a(t_2 - t_1)] [I_X + K_{x,z} I_Z]$$

and

$$B_Z = v_Z K_z [K_a(t_2 - t_1)] [I_Z + K_{z,x} I_X]$$

The terms Δmv_X and Δmv_Z are defined as the difference between the strain-gage bridge output at the test point and the average of the bridge output during static loading. For the second and subsequent load iterations:

$$L_X = \frac{\Delta mv_X - B_X}{v_X K_x [1 + K_a(t_2 - t_c)]} + K_{x,z} I_Z + [1 + K_b(t_2 - t_c)] K_{x,xz} I_X I_Z$$

$$-K_{x,z}(L_Z + I_Z) - [1 + K_b(t_2 - t_c)] K_{x,xz}(L_X + I_X)(L_Z + I_Z)$$

and

$$L_Z = \frac{\Delta mv_Z - B_Z}{v_X K_x [1 + K_a(t_2 - t_c)]} + K_{z,x} I_X + [1 + K_b(t_2 - t_c)] K_{z,xz} I_X I_Z$$

$$- K_{z,x}(L_X + I_X) - [1 + K_b(t_2 - t_c)] K_{z,xz}(L_X + I_X)(L_Z + I_Z)$$

These forces are calculated for each data point over a 30-sec period and then an average is taken for the entire sample of approximately 150 points. Each test sample is begun only after all of the aircraft and CCW operating parameters have attained a stable condition. Although these aircraft parameters and hence the loads are not truly static, the variation is small during the sample period. This procedure of averaging the large number of data points acquired during the sample period has yielded results that are generally repeatable within ±0.05% of the maximum measured forces.

Data system resolution — The data system divides the range of each parameter into 1,024 parts, or counts, in order to digitally transmit the analog signals from its individual measuring devices. The effect of this digitization is to create discrete increments in the transmitted value of each parameter that are a constant percentage of its full-scale range. Since the input signal may cover any value in the parameter's range, the incoming signal often will be between discretes or counts, and, hence, the next higher or lower value will be output into the data stream. In the case of the load pads during the current test, this discrete increment was about 222 N (50 lb). Averaging a statistically meaningful sample of data tends to minimize the error introduced by these fluctuations, particularly under truly static conditions. For example, it was possible to tell if the aircraft crew members were at their proper stations (static measurements were not accomplished until they were). In addition, aircraft weight calculations based on load-pad readings were compared with weight readings measured with standard weight scales and were found to correlate within 0.10%.

Small loads — Although the load pads and data system give highly accurate results with large loads, some problems occurred when the loading was very low. When the loads are approximately the same level as the increment value, 222 N (50 lb), the recorded values can vary by approximately ±100% from the true value. This has a varying effect that depends on the type of load input and direction of loading. The major effect of this problem on the present program was that it made it impossible to measure CCW trailing edge turning without the USB engine running; as a result, no baseline CCW trailing edge data are presented.

CCW TRAILING EDGE CALCULATIONS

The individual pressures and temperatures from the CCW plenum and the USB trailing-edge pressure were sampled by the aircraft data system, displayed in real-time, and recorded for later processing. These parameters were sampled for 30 sec after they were stabilized on a test condition, at a sample rate of five points per second. The individual plenum temperatures and pressures were averaged for the data analysis.

CCW jet velocity — the jet velocity was calculated assuming an isentropic expansion from CCW plenum total conditions to free-stream static conditions:

$$V_j = a_j M_j = (\gamma R g T_j)^{1/2} M_j = \left\{ 2gRT_d \frac{\gamma}{\gamma - 1} \left[1 - \left(\frac{P_\infty}{P_d} \right)^{\frac{\gamma - 1}{\gamma}} \right] \right\}^{1/2}$$

It is realized that expansion to local static conditions at the jet exit gives a far more realistic value of V_j and that expansion to free-stream static pressure underestimates V_j and M_j. However, local exit conditions are functions of local geometry — and thus a comparison of two blown airfoils of unlike trailing-edge geometry but with identical slot areas, plenum pressures, and temperatures — would yield

ORIGINAL PAGE IS
OF POOR QUALITY

unlike values of momentum coefficient. The momentum coefficient based on expansion to free-stream conditions is thus accepted as a more "universal" parameter for comparison of blown systems.

CCW slot mass flow — The mass flow to the CCW slot was provided by two aircraft ground-air-supply carts. Because these carts are used daily for aircraft servicing, it was not possible to modify them to accurately measure their mass flow. Hence, the mass flows used in this analysis were calculated for isentropic conditions as follows:

Choked flow:

$$\dot{m}_j = A_j P_d \sqrt{\frac{\gamma}{R g T_d}} \left(\frac{2}{\gamma+1}\right)^{\frac{\gamma+1}{2(\gamma-1)}}, \quad P_d/P_\infty \geq 1.89$$

Unchoked flow:

$$\dot{m}_j = A_j P_d \left\{ \frac{2\gamma}{(\gamma-1) R g T_d} \left[\left(\frac{P_\infty}{P_d}\right)^{2/\gamma} - \left(\frac{P_\infty}{P_d}\right)^{\frac{\gamma+1}{\gamma}} \right] \right\}^{1/2}$$

This mass calculation requires values of expanded slot height as a function of plenum pressure in order to accurately determine the CCW nozzle area, A_j. This slot height is a function of both the plenum temperature and pressure, as noted earlier. Based on limited measurements, an extrapolated variation of the nozzle slot height is shown in figure 16 for the two nominal cold slot heights of 0.102 cm (0.040 in.) and 0.051 cm (0.020 in.), respectively. The slot height values from this curve were used to make the momentum flux calculation contained in this report.

AIRCRAFT EQUATIONS

The locations and directions of the forces acting on the aircraft are shown in figure 17.

Net axial force — The net axial force is the sum of the axial forces measured by the load pads, corrected by the wind ram drag.

$$F_X = L_{X_1} + L_{X_2} + L_{X_3} + \frac{\dot{w}_a}{g} V_w \cos \theta_w$$

Note: If θ_w is greater than 90° or less than -90° then the ram drag term is set equal to zero.

Net lift — The net lift force on the aircraft is the sum of vertical forces as measured by the load pads corrected for the fuel used.

$$F_Z = L_{Z_1} + L_{Z_2} + L_{Z_3} - W_{fuel}$$

where

$$W_{fuel} = G_{fuel}\,\rho_{fuel}$$

Resultant force — The resultant force is

$$F_R = \left(F_Z^2 + F_X^2\right)^{1/2}$$

and the resultant angle is

$$\theta_R = \tan^{-1}(F_Z/F_X)$$

Referred parameters — The measured forces and engine parameters are corrected or referred to sea level standard day values in order to permit direct comparisons with other data from previous tests. The measured forces are corrected by the ratio of ambient barometric pressure to standard day sea level pressure; hence, the referred force = measured force/(P_∞/P_{ref}). Similarly, the measured fan speed is corrected by the square root of the ratio of the ambient temperature to standard day temperature expressed in degrees Kelvin or Rankine:

$$N_{1_{referred}} = N_{1_{measured}} \sqrt{\theta}; \text{ where } \theta = \frac{T_\infty}{T_{ref}}$$

RESULTS AND DISCUSSION

Data from references 1-3 imply that CCW/USB thrust deflection is primarily a function of engine thrust level and characteristics of the CCW jet (principally jet pressure and momentum). These parameters were thus of prime concern in the present investigations.

Thrust level — Figures 18 and 19 present resultant thrust levels, produced by different amounts of CCW blowing, as functions of engine installed thrust and power setting (percent fan rpm). In these data, installed thrust is the static thrust of the YF-102 engine as installed in the QSRA nacelle on the wing, with D-nozzle and vortex generators, and USB flaps set at zero deflection, and as recorded during run 6 (pts 110-129) of the present investigation. Resultant thrust is determined from vertical and horizontal balance readings only, since the side-force component cannot be measured on the load pads. Thus, spanwise thrust components are not included in installed or resultant thrust measurements.

Deflection angle - The resulting thrust-deflection angles as functions of the installed thrust for a nominal CCW slot height of 0.102 cm (0.040 in.) are compared with the conventional USB flap at zero deflection in figure 20. Trailing-edge camber produced by addition of the CCW device, with no blowing, yielded increases in thrust turning-angle, over the basic flap, of from 7° to 20°, depending on thrust level. The addition of blowing produced thrust deflection angles up to 97° at low thrust settings, and 40° at maximum thrust. The same data are plotted in terms of resultant thrust for $h = 0.102$ cm (0.040 in.) in figure 21, and $h = 0.051$ cm (0.020 in.) in figure 22.

Figure 19 implies that the resultant thrust at a constant power setting is reduced with increasing blowing pressure. However, as can be seen from figure 20, the USB jet is also being turned through a greater angle as blowing pressure

ORIGINAL PAGE IS
OF POOR QUALITY

increases. This USB jet is not a uniform thin sheet, but is actually three-dimensional, with varying thickness and velocity both along and above the CCW span. There is usually some loss in efficiency when turning this jet, with losses increasing with angle for the conventional USB flap. It is assumed that a similar mechanism is affecting the CCW/USB jet turning. This thrust loss could prove advantageous on STOL approach, where reduced thrust at high lift allows steeper glide slopes, but may have an adverse effect under flight conditions that require maximizing thrust (waveoff).

CCW jet momentum – Combining figures 21 and 22 shows increasing thrust-turning with increasing CCW jet momentum; however, slot height variation produces relatively little effect, other than in the pressure required to produce a given momentum as slot area changes. These curves are nearly linearized by plotting against engine exhaust Mach number near the CCW slot instead of resultant thrust, as shown in figures 23 and 24. Figure 25 is a cross plot of figure 21 and shows thrust-turning, as a function of the momentum required to produce it, in terms of a percentage of installed thrust. Figure 25 is an indication of engine bleed requirements for an installed on-board system that would replace the air-start carts.

The potential for efficient STOL operation of the CCW-USB system is shown in figure 26, where the horizontal and vertical thrust components are plotted for various blowing levels. Addition of aerodynamic lift and drag would convert these to lift-drag polars, shifting all curves upward and to the left (or drag) side of the plot. Operation in flight at a constant vertical (or lift) force could be maintained, while horizontal force was being converted from low- to high-thrust recovery by decreasing blowing, thus representing conversion from a landing to a wave-off mode. These operations are possible without change in angle of attack, and require no deflections of moving parts in the high-lift system.

A visualization of the CCW flow-turning is provided in figure 27, where the flow field on the surface of the CCW trailing edge is mapped by tufts. These tufts are seen to turn to a nearly horizontal position, heading forward. Evidence that large portions of the engine exhaust were entrained to large deflections was observed in motions of the grass behind the aircraft: it waved violently in the exhaust when blowing was off, but became still as blowing increased. At higher blowing, objects on the ground below and ahead of the CCW trailing edge became violently disturbed.

Thrust comparison – Figure 28 compares thrust-turning results from figure 21 with predicted results based on model-scale data taken from reference 3. These model results were scaled up based on the parameters $T_{installed}/A_{noz}$ and $\dot{m}V_j/A_{noz}$, where A_{noz} is the engine D-nozzle effective exhaust area. The predicted thrust-turning angle is slightly greater than that measured for the higher blowing case, but less than that measured at lower blowing. Several factors relative to this performance, noted during the investigations, will provide guidance in the development of future configurations. The CCW slot upper lip did not produce a jet slot that excited tangentially to the round trailing edge, but instead intersected the radius ahead of and below the tangency point. This can cause loss of jet static pressure differential and less than optimum jet entrainment and turning. Experience has shown that at higher pressures, complete detachment of the jet can occur if the geometry is sufficiently misaligned. Secondly, the full-scale CCW/USB bolt-on aluminum assembly was distorted when it was exposed to starter-cart supply temperatures of 177°C-188°C (350°F-370°F), as measured in the plenum. This distortion of the very thin upper slot lip could have produced a non-uniform spanwise slot height distribution, as well as slot heights larger than anticipated. Reference 9 indicates that large slot heights at high jet pressures can produce serious deficiencies in jet turning, or

ORIGINAL PAGE IS
OF POOR QUALITY

even cause complete jet detachment. Both of these factors imply that full-scale turning was penalized by trailing-edge geometry at higher blowing pressure.* Based on the lower pressure data, it would appear that full-scale thrust deflection at the 2.089×10^5 Pa (30.3 psig) blowing pressure can possibly exceed the predicted values of figure 28, using the experience gained during these tests to improve trailing-edge geometry or CCW/USB integration.

CONCLUDING REMARKS

Full-scale thrust-deflection investigations have been conducted on the QSRA to determine the effectiveness of the CCW/USB concept in turning engine thrust pneumatically, with no mechanical moving parts to control deflection angle. These test results compared favorably with those from small-scale model investigations conducted by DTNSRDC using a cold-jet propulsion simulator. Full-scale variations in engine-thrust level, CCW blowing pressure, and CCW slot height have led to the following comments:

1. A CCW pressure of 2.089×10^5 Pa (30.3 psig) [≈1.82 kg/sec (4 lbs/sec) slot weight flow] produced static thrust deflection angles ranging from 40° to 97°, depending on thrust level. For a given power setting and as thrust turning was increased, there was some reduction in resultant thrust values.

2. Variation in the nominal CCW slot height setting had relatively little effect on thrust-turning other than in the pressure required to produce a given slot momentum.

3. In general, the CCW-USB system was able to pneumatically produce engine-thrust deflection values similar to those produced by a large mechanical USB flap behind a turbofan engine at the lower thrust levels.

4. Thrust-turning values higher than those recorded at 2.089×10^5 Pa (30.3 psig) pressure may be possible with an improved second generation CCW/USB test article. For this test, CCW duct air pressures were obtained from two engine-start carts external to the aircraft. Higher pressures, and thus greater thrust turning, could be obtained when the system is fully integrated with the on-board engines. Therefore, thrust-turning of the order of that measured during wind-tunnel tests should be achievable in actual practice.

5. The potential for a full CCW/USB system, as suggested in references 1-3, has now been further demonstrated under full-scale conditions. The CCW, which would be employed as a no-moving-parts (ref. 4) high-lift/high-drag device outboard of the engines, has been proved on the A-6 aircraft (refs. 5 and 6). The inboard pneumatic thrust deflection system using the CCW with USB has been demonstrated statically in the current tests.

The feasibility of this CCW/USB system for STOL operations is due to its versatility in controlling horizontal forces to produce either thrust or drag while maintaining a constant large vertical force. These forces are controlled by changing the amount of blowing, either inboard or outboard or both, thus allowing rapid readjustment of the spanwise circulation and of the load distribution on the wing. Depending

---

*Also, as mentioned earlier, vortex generators in the exhaust and a CCW span less than the width of the exhaust both degrade CCW thrust turning.

on mission requirements, this system could have significant advantages over a mechanical flap design. For instance, an advanced CCW/USB pneumatic control system could be used on a high-speed fighter to provide substantially increased maneuverability without conventional control-surface speed boundaries; and the system's use on a super-STOL would make it possible to trade maximized acceleration during the initial takeoff run for high lift at rotation. The transition from landing to wave-off configurations could be achieved almost instantaneously by changing blowing pressure in the ducts, a procedure that does not require moving any external parts.

Additional static investigations are planned that will evaluate engine thrust-turning with hardware improvements and with a smaller trailing-edge radius. This alternative trailing-edge radius will have a low cruise drag, thereby allowing a no-moving-parts thrust-deflection/reversal system which will further increase system simplicity. The ultimate test will be a flight demonstration of this CCW/USB thrust deflecting-system.

REFERENCES

1. Nichols, J. H., Jr.; and Englar, R. J.: Advanced Circulation Control Wing System for Navy STOL Aircraft. AIAA Paper 80-1825, Anaheim, Calif., 1980.

2. Nichols, J. H., Jr.; et al.: Experimental Development of an Advanced Circulation Control Wing System for Navy STOL Aircraft. AIAA Paper 81-0151, St. Louis, Mo., 1981.

3. Harris, M. J.: Investigation of the Circulation Control Wing/Upper Surface Blowing High Lift System on a Low Aspect Ratio Semispan Model. Report ASED-81/10, David Taylor Naval Ship Research and Development Center Bethesda, Md., May 1981.

4. Englar, R. J.: Low-Speed Aerodynamic Characteristics of a Small Fixed-Trailing-Edge Circulation Control Wing Fitted to a Supercritical Airfoil. Report ASED-81/08, David Taylor Naval Ship Research and Development Center, Bethesda, Md., Mar. 1981.

5. Englar, R. J. et al.: Design of the Circulation Control Wing STOL Demonstrator Aircraft. AIAA Paper 79-1842, New York, N.Y., 1979. (Republished in AIAA Journal of Aircraft, vol. 18, no. 1, Jan. 1981, pp. 51-58.)

6. Pugliese, A. J.; and Englar, R. J.: Flight Testing the Circulation Control Wing. AIAA Paper 79-1791, New York, N.Y., 1979.

7. Eppel, J. C.: Quiet Short-Haul Research Aircraft Familiarization Document, Revision 1. NASA TM-81298, 1981.

8. Shovlin, M. D.; Skavdahl, H.; and Harkonen, D. L.: Design and Performance of the Propulsion System for the Quiet Short-Haul Research Aircraft (QSRA). AIAA Paper 79-1313, Las Vegas, Nev., 1979. (Republished in AIAA Journal of Aircraft, vol. 17, no. 12, Dec. 1980, pp. 843-850.)

9. Englar, R. J.: Experimental Investigation of the High Velocity Coanda Wall Jet Applied to Bluff Trailing Edge Circulation Control Airfoils. Report 4708, David Taylor Naval Ship Research and Development Center, Bethesda, Md., Sept. 1975.

Figure 1. Quiet Short-Haul Research Aircraft.

ORIGINAL PAGE
BLACK AND WHITE PHOTOGRAPH

Figure 2. A-6/CCW Flight Demonstrator Aircraft.

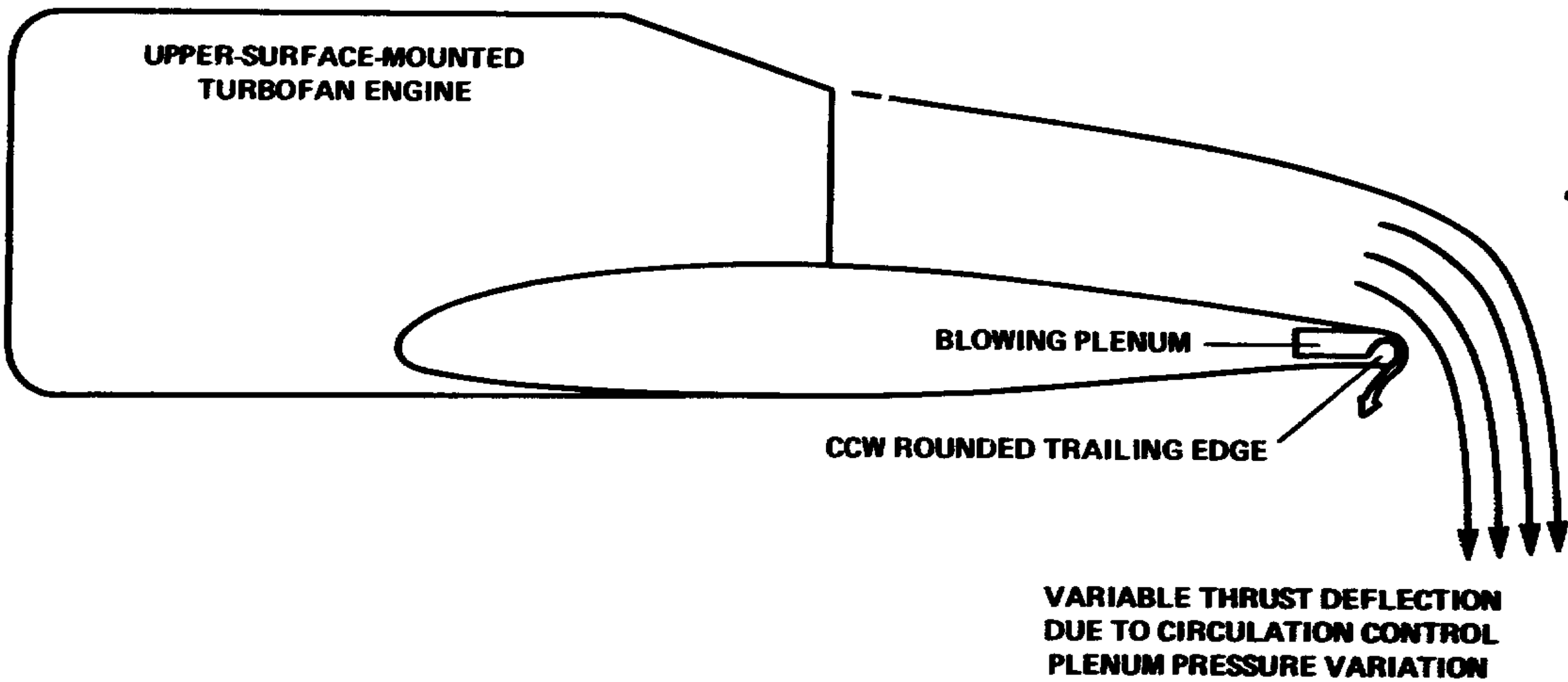

Figure 3. CCW/USB thrust deflector and lift augmentation concept.

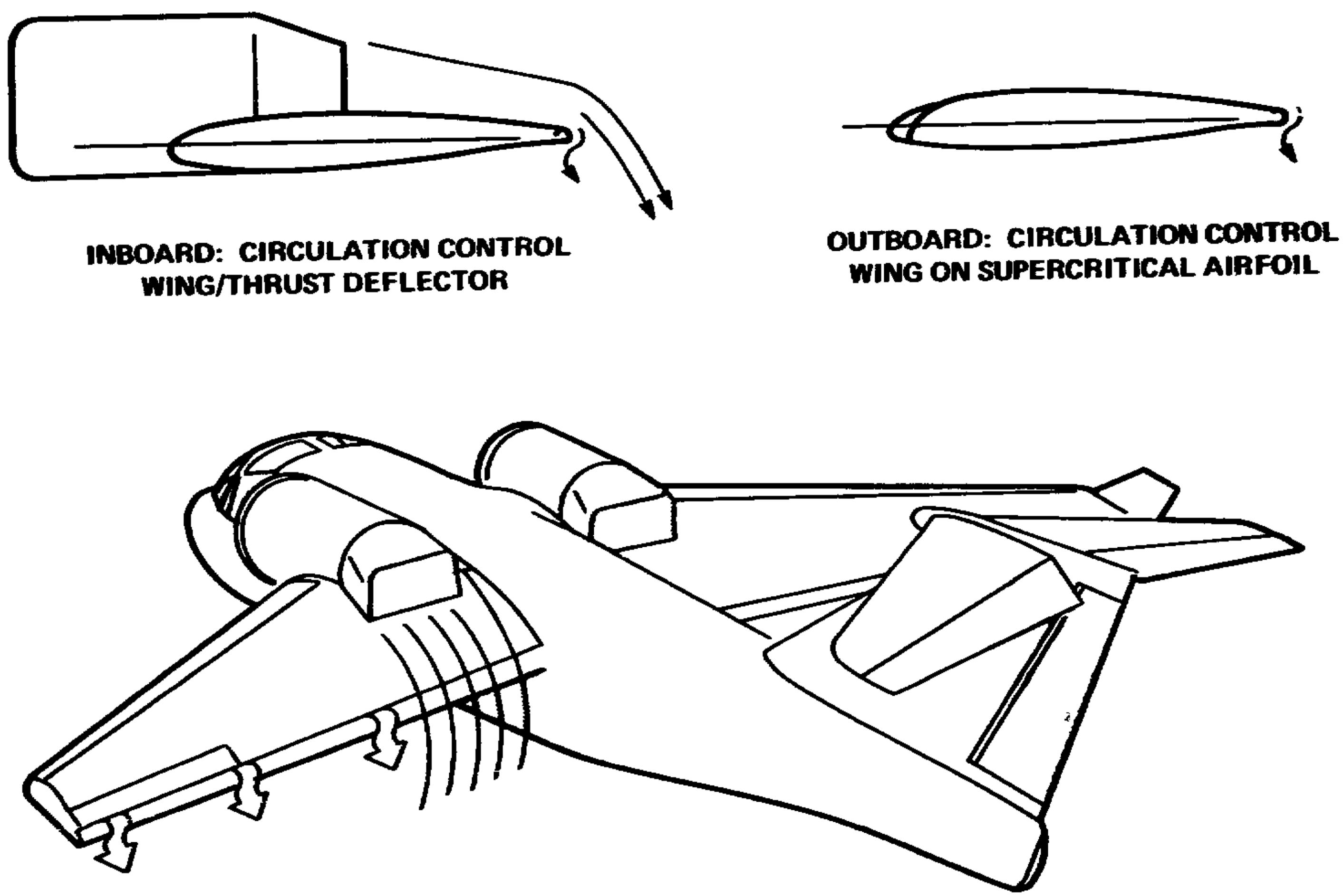

Figure 4. CCW and CCW/USB STOL aircraft proposed by DTNSRDC.

ORIGINAL PAGE IS
OF POOR QUALITY

AERODYNAMIC DATA

	WING	HORIZ	VERT
AREA (TRAP), ft^2	600.0	233.0	152.0
SPAN, ft	73.5	32.0	14.0
ASPECT RATIO	9.0	4.4	1.22
TAPER RATIO	0.30	0.75	0.60
SWEEP, C4, deg	15.0	3.0	18.0
M.A.C. in.	107.4	88.0	137.0
CHORD ROOT, in.	150.7	100.0	168.0
CHORD TIP, in.	45.2	75.0	100.0
T/C BODY SIDE, %	18.54	14	14
T/C TIP, %	15.12	12	14
INCIDENCE, deg	4.5	–	–
DIHEDRAL, deg	0.0	–	–
TAIL ARM, in.	–	525.0 in.	488.0 in.
VOL COEFF V	–	1.098	0.1402

CONTROL SURFACES

ft^2/APL *		BLOWN
AILERON	32.2	BLC
FLAPS INBD	105.0	USB
FLAPS OUTBD	40.2	NONE
SPOILERS	33.7	NONE
L.E. FLAPS	54.3	NONE
ELEVATOR	81.6	NONE
RUDDER	60.8	NONE

*THEORETICAL RETRACTED AREA

PROPULSION

ENGINE	LYCOMING YF-102
STATIC THRUST	6225**
FAN P.R.	1.45
BY-PASS RATIO	6.0

**MEASURED THRUST

LANDING GEAR

GEAR	STROKE	TIRE	TIRE O.D.	ROLLING R.
MLG, in.	21.0	14x15	37	~ 15.2
NLG, in.	17.5	8.90-12.50 TYPE III	27.5	12.0

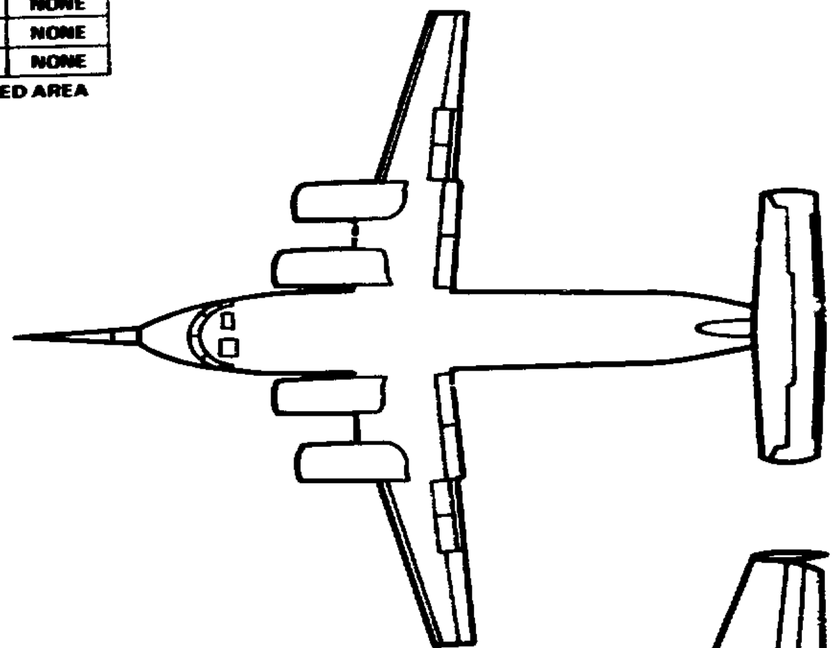

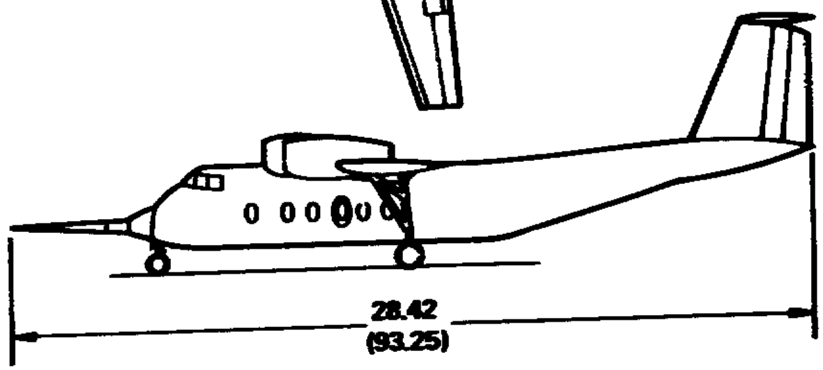

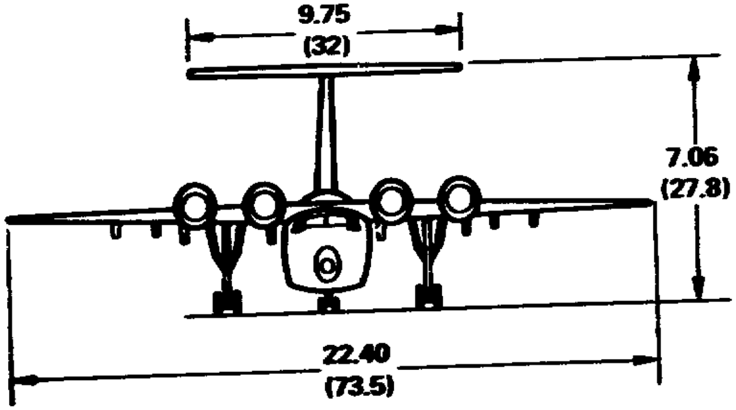

DIMENSIONS IN m(ft)

Figure 5. QSRA design and configuration data.

ORIGINAL PAGE IS
OF POOR QUALITY

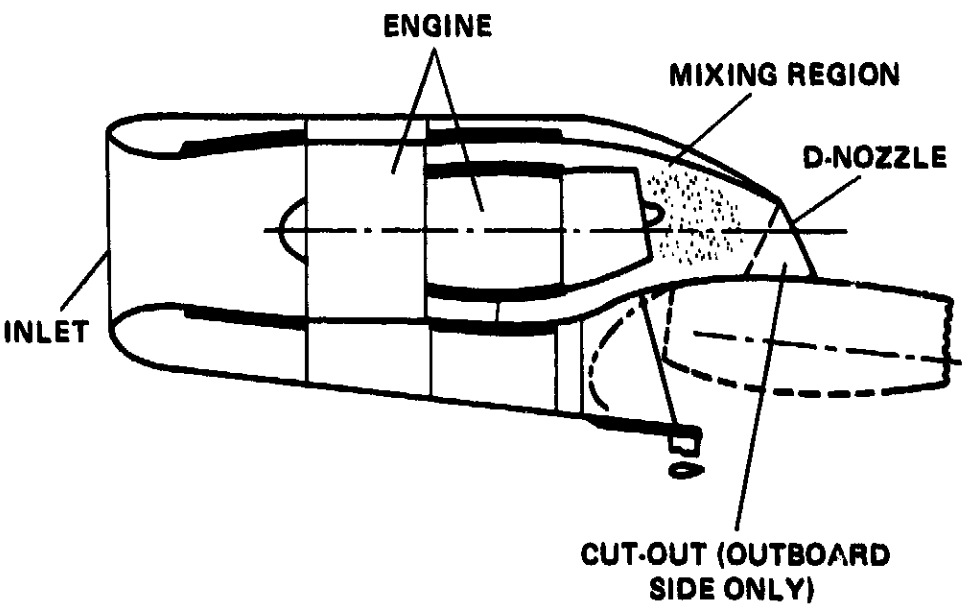

Figure 6. QSRA nacelle.

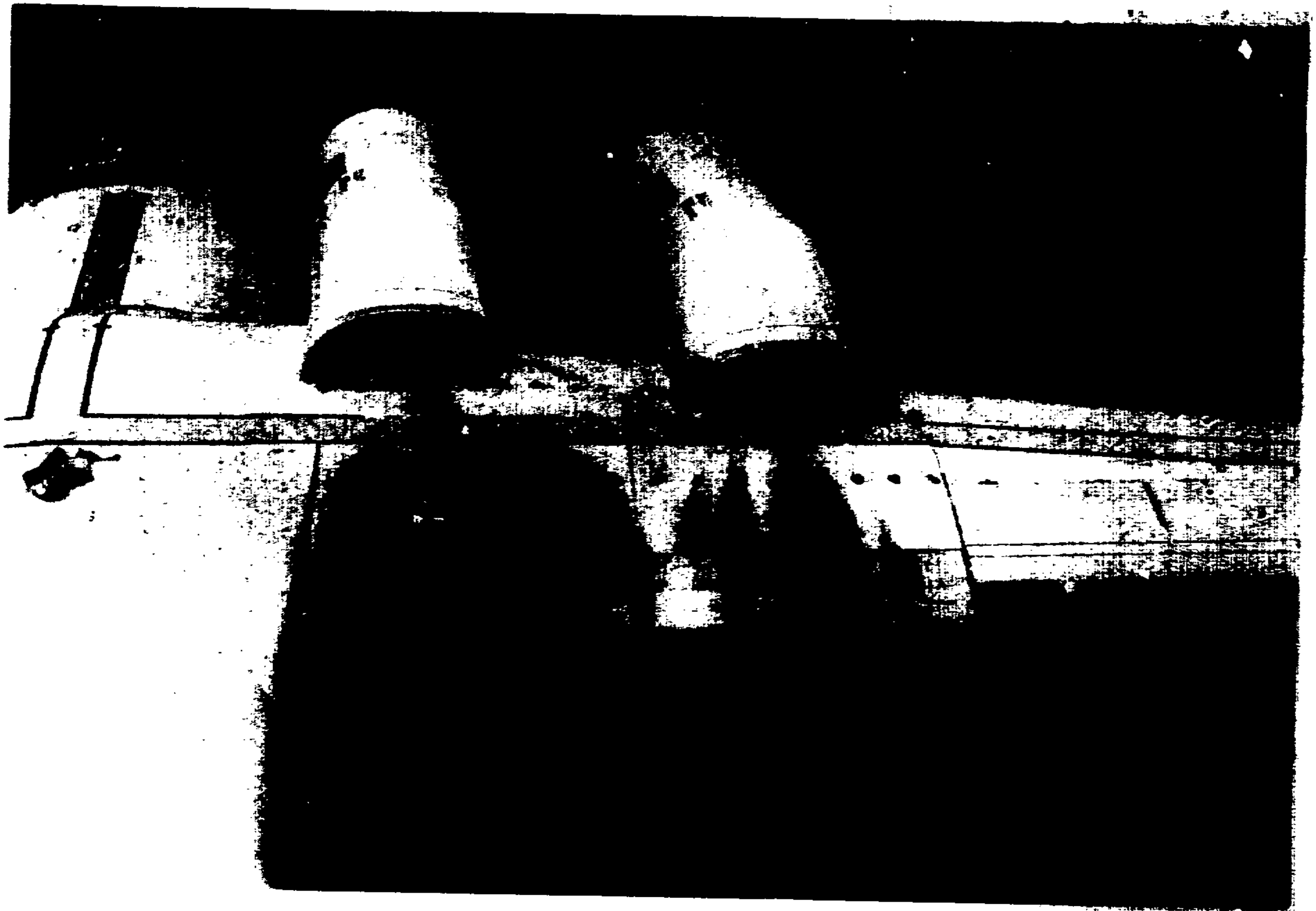

Figure 7. Topview of QSRA showing engine nozzle cutouts and vortex generators.

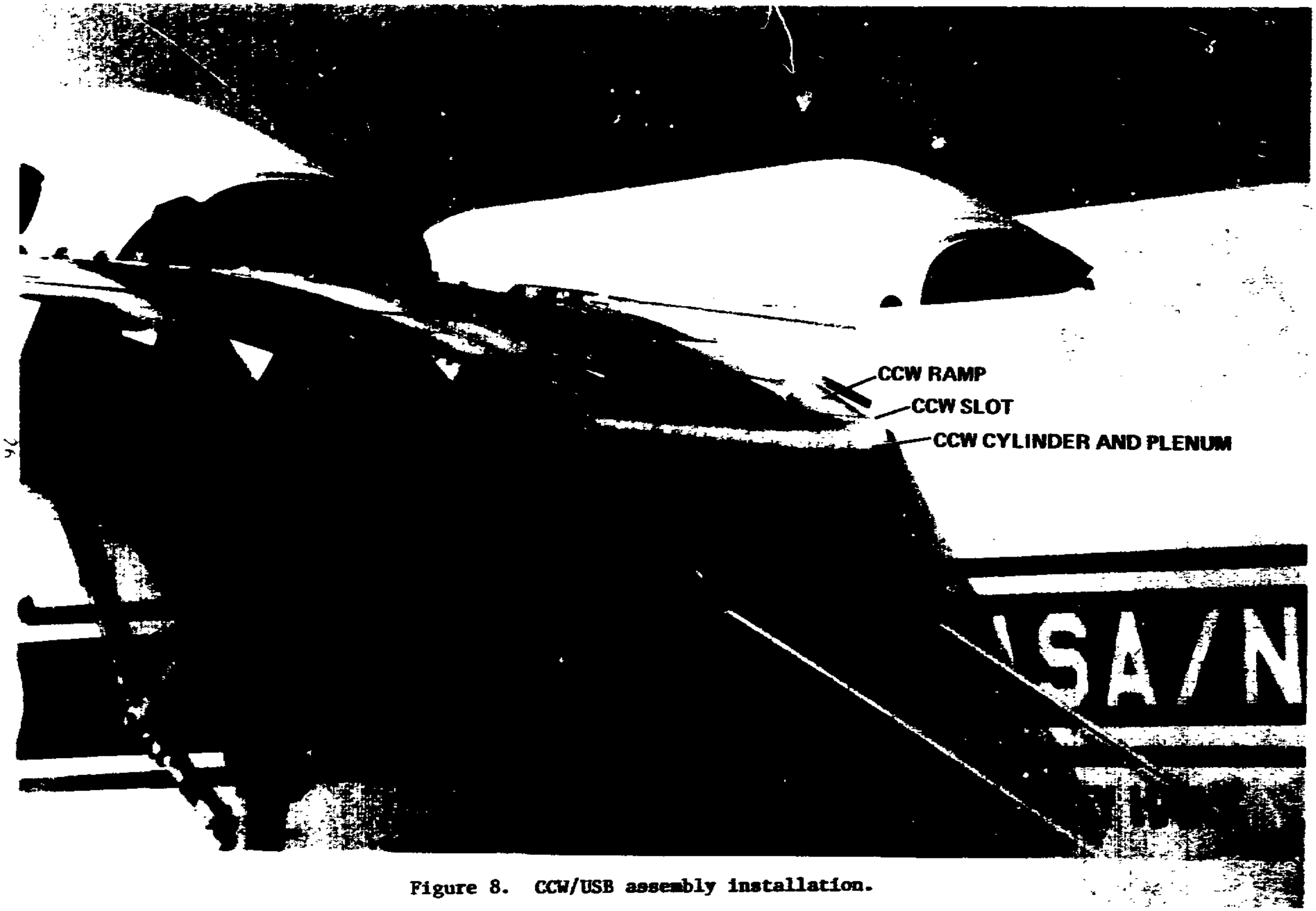

Figure 8. CCW/USB assembly installation.

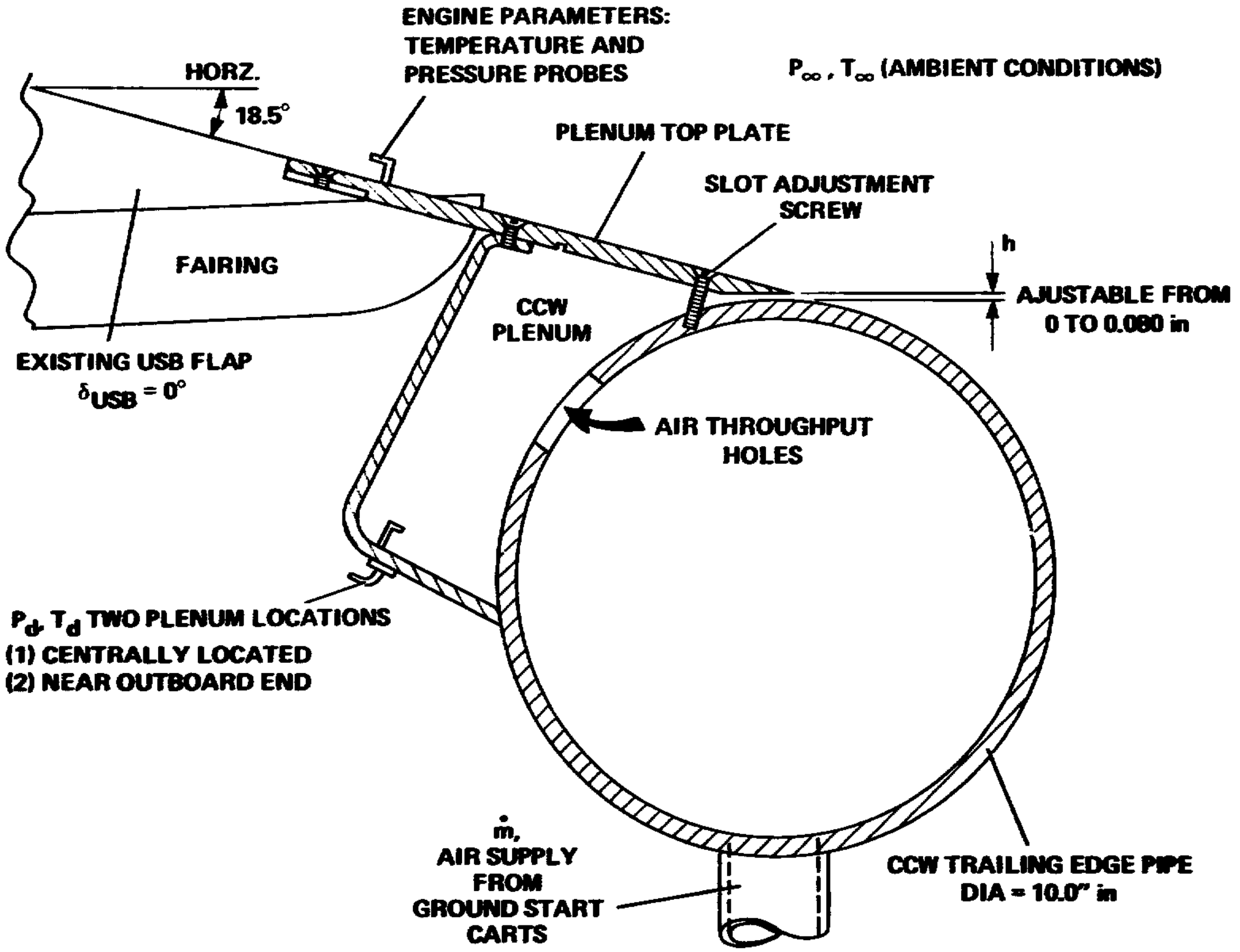

ORIGINAL PAGE IS
OF POOR QUALITY

Figure 9. Detail drawing of circulation control wing (CCW) trailing edge.

ORIGINAL PAGE
BLACK AND WHITE PHOTOGRAPH

ected to air supply hoses.

ORIGINAL PAGE IS
OF POOR QUALITY

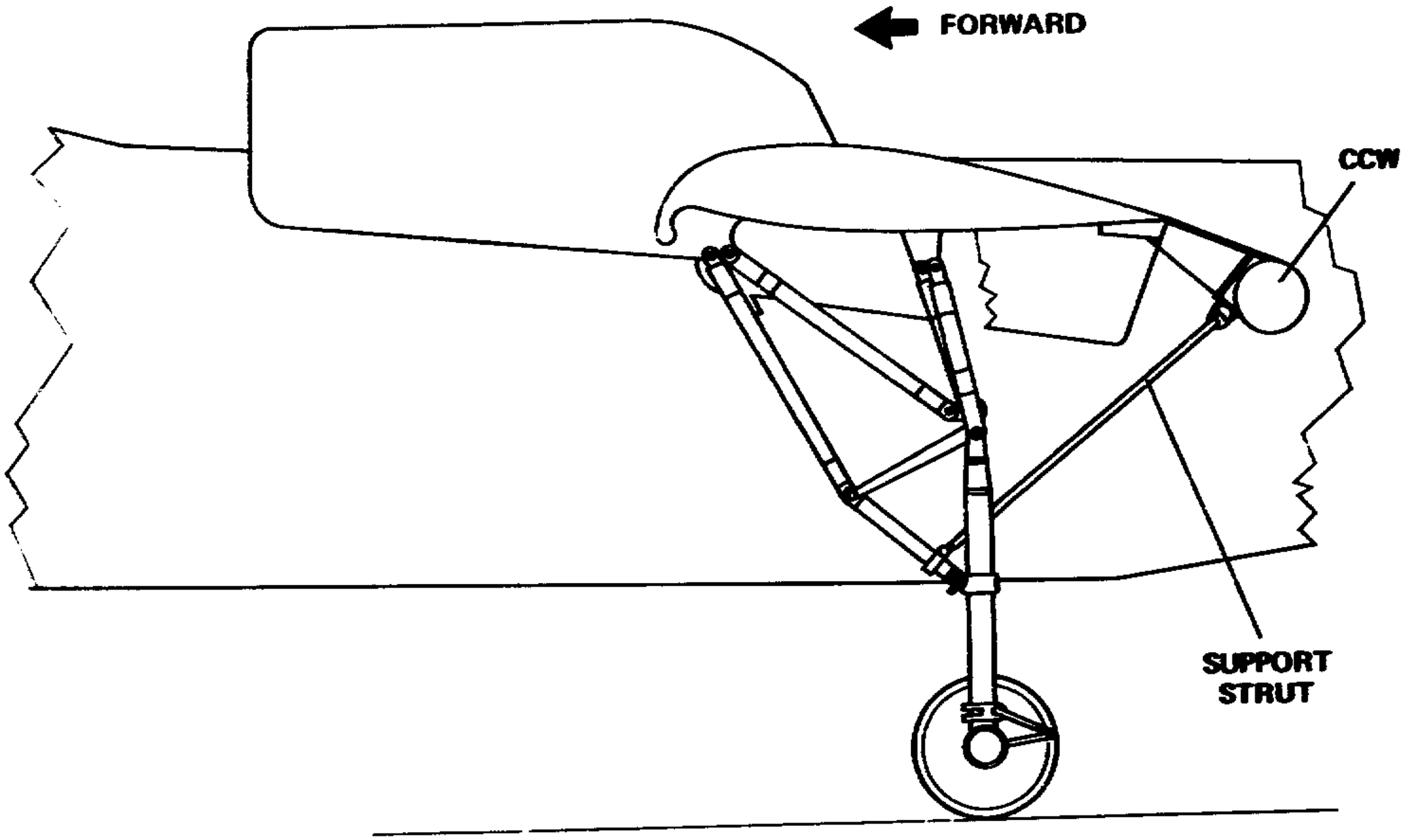

Figure 11. Drawing of CCW installed on QSRA.

ORIGINAL PAGE
BLACK AND WHITE PHOTOGRAPH

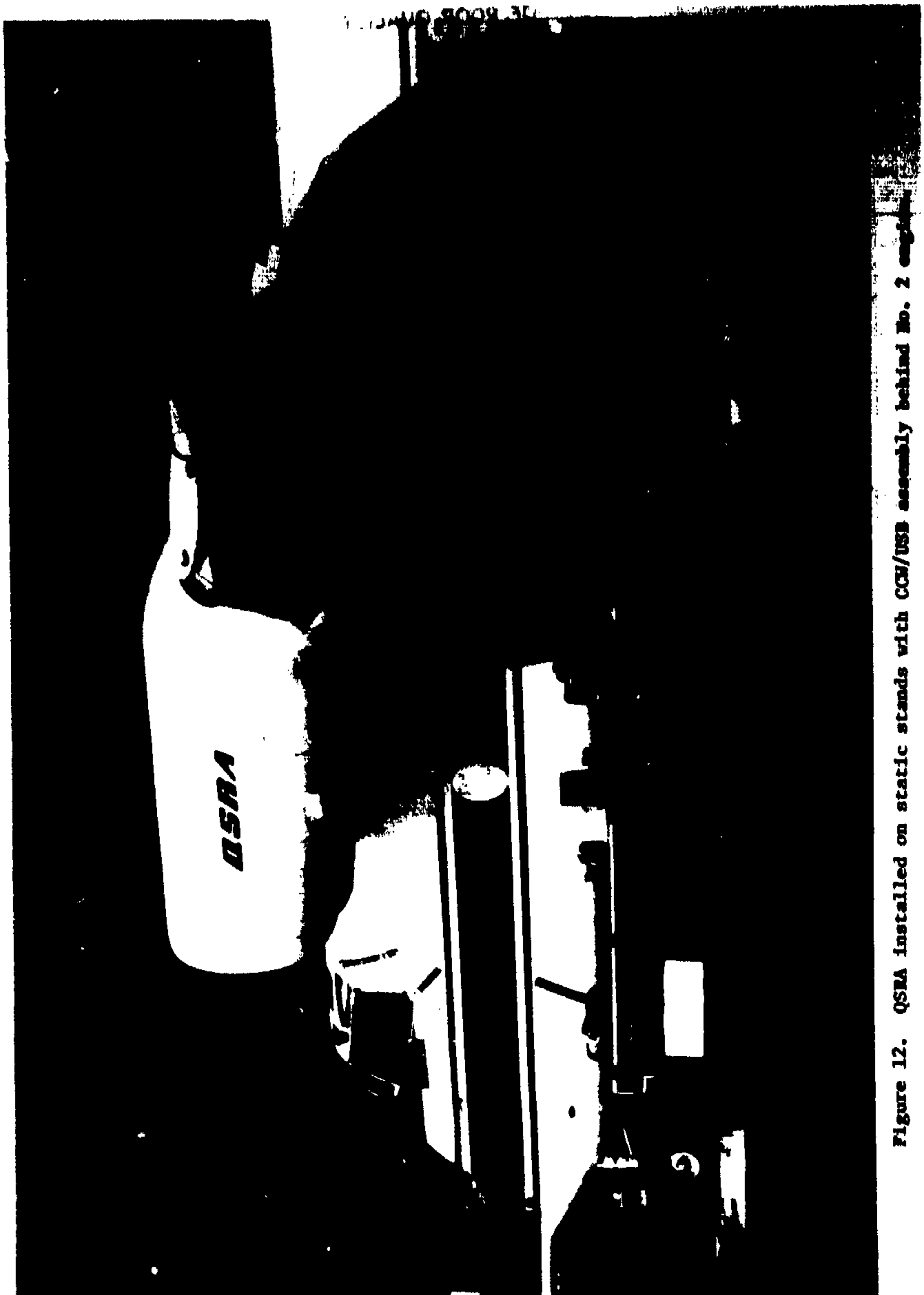

Figure 12. QSRA installed on static stands with CCW/USB assembly behind No. 2 engine.

ORIGINAL PAGE
BLACK AND WHITE PHOTOGRAPH

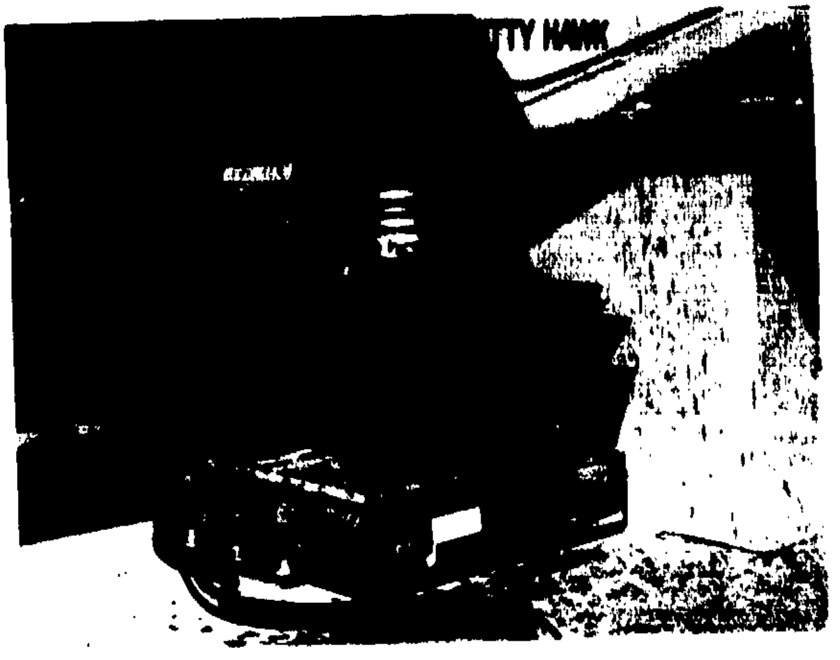

(a) Left main gear.

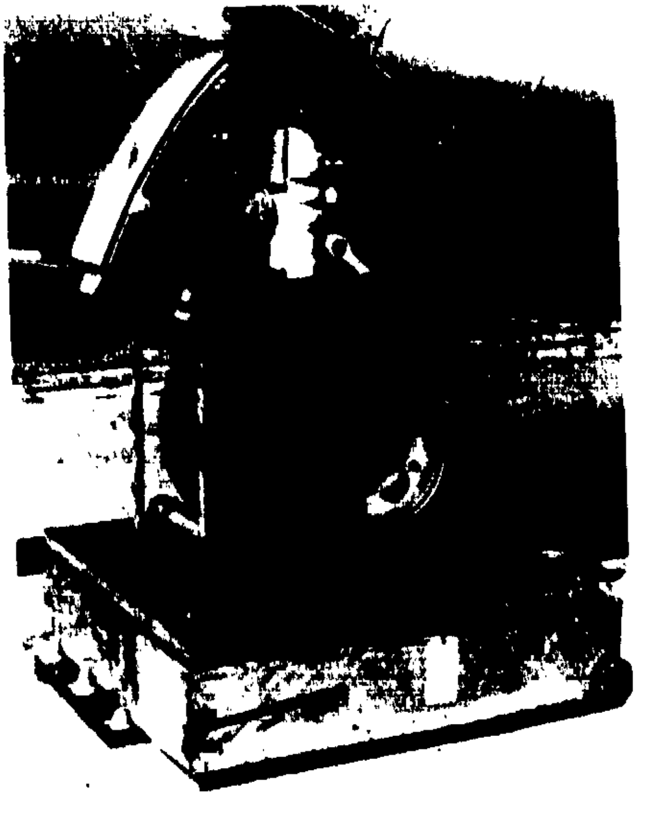

(b) Nose gear.

Figure 1[illegible]. Gears installed on load pads.

ORIGINAL PAGE
BLACK AND WHITE PHOTOGRAPH

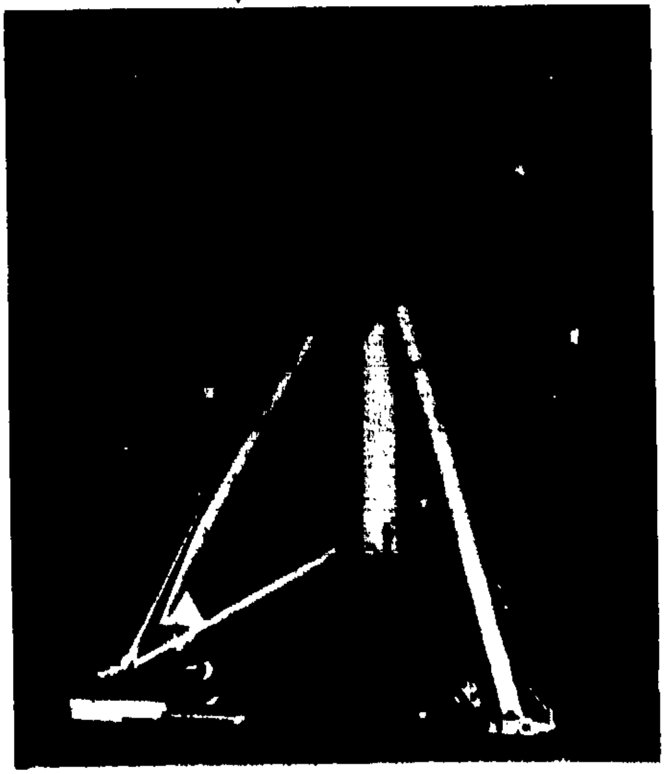

Figure 14. Weather station.

Figure 15. Technicians adjusting CCW slot.

ORIGINAL PAGE IS
OF POOR QUALITY

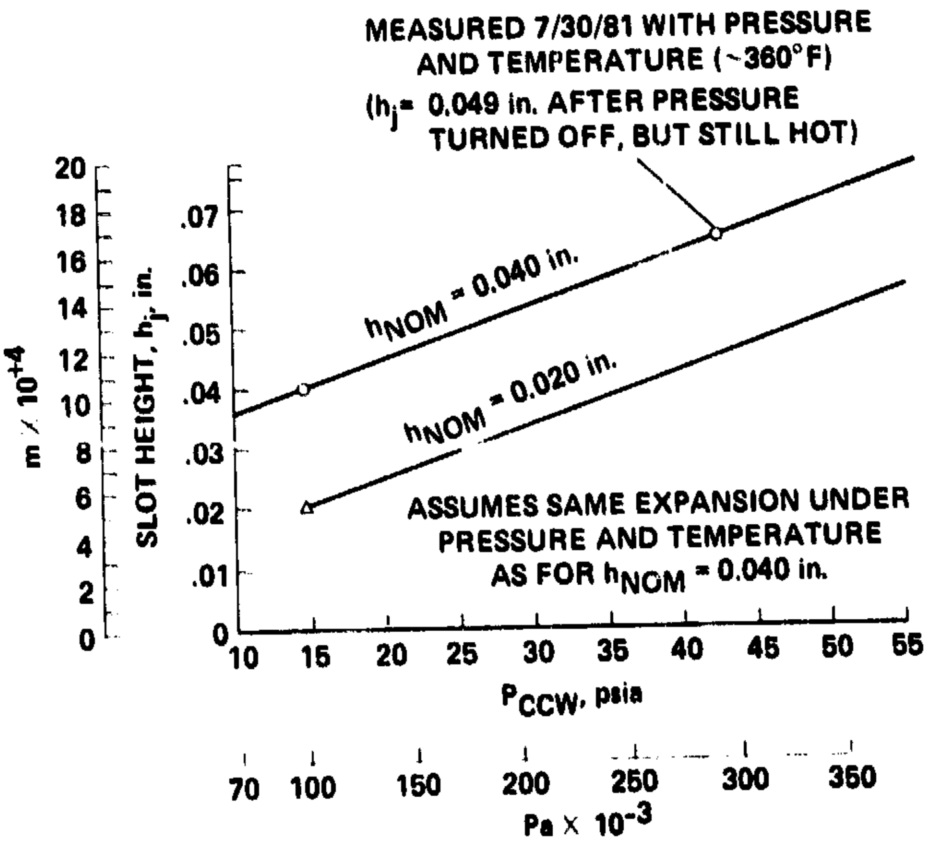

Figure 16. QSRA CCW/USB measured and extrapolated CCW slot height.

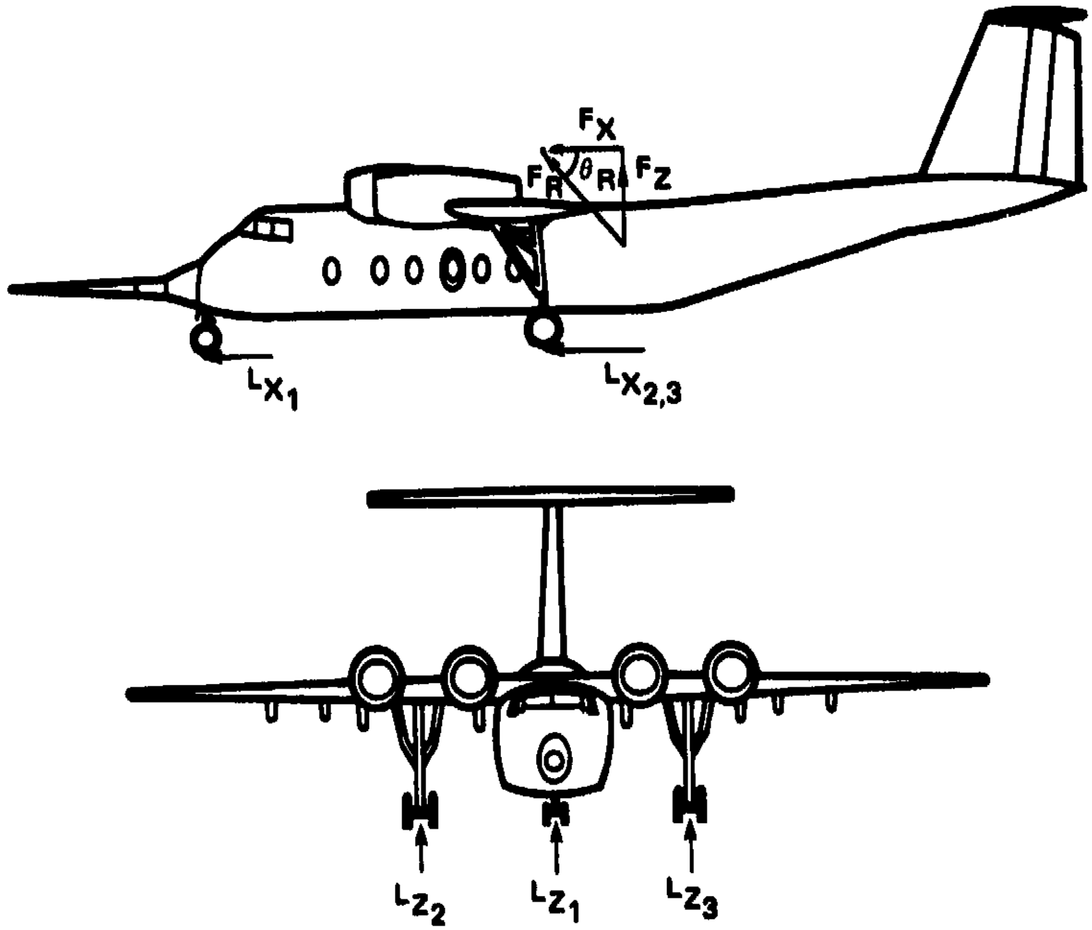

Figure 17. Location and direction of forces acting on aircraft.

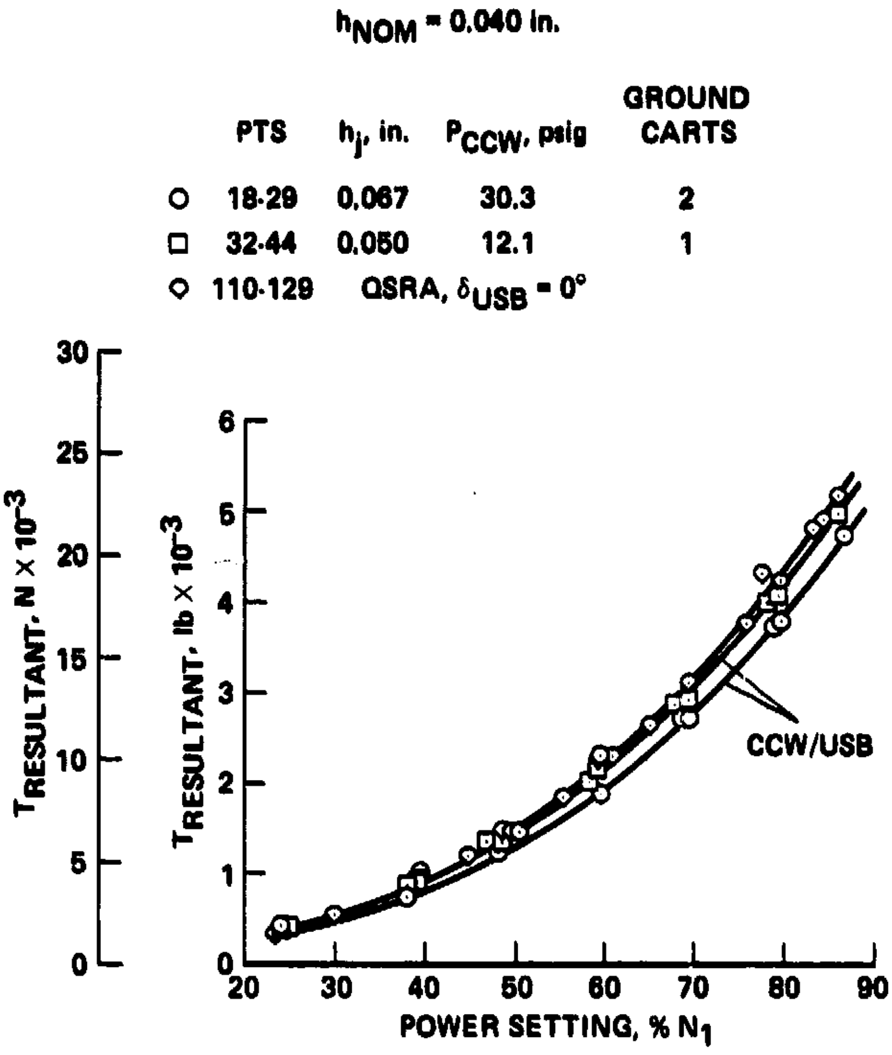

Figure 18. CCW/USB Power setting vs. resultant thrust.

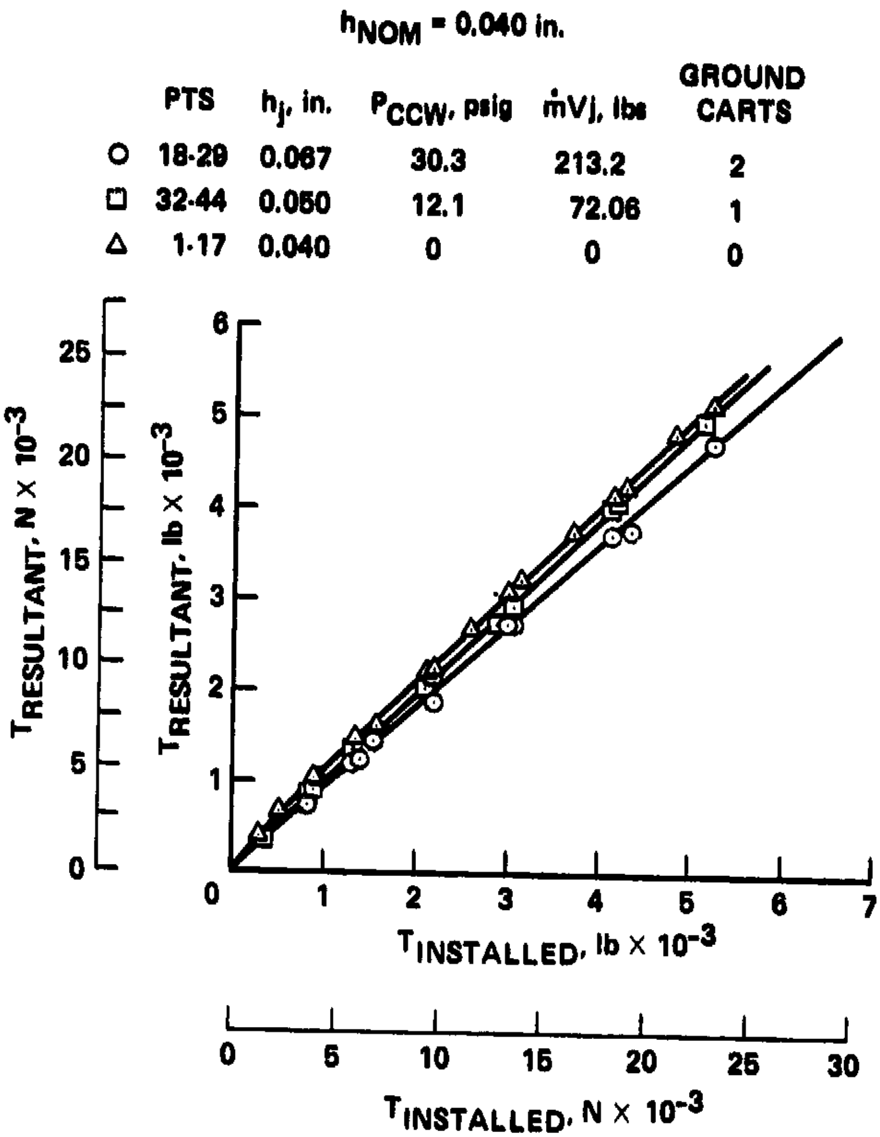

Figure 19. QSRA CCW/USB Static thrust, installed vs. resultant.

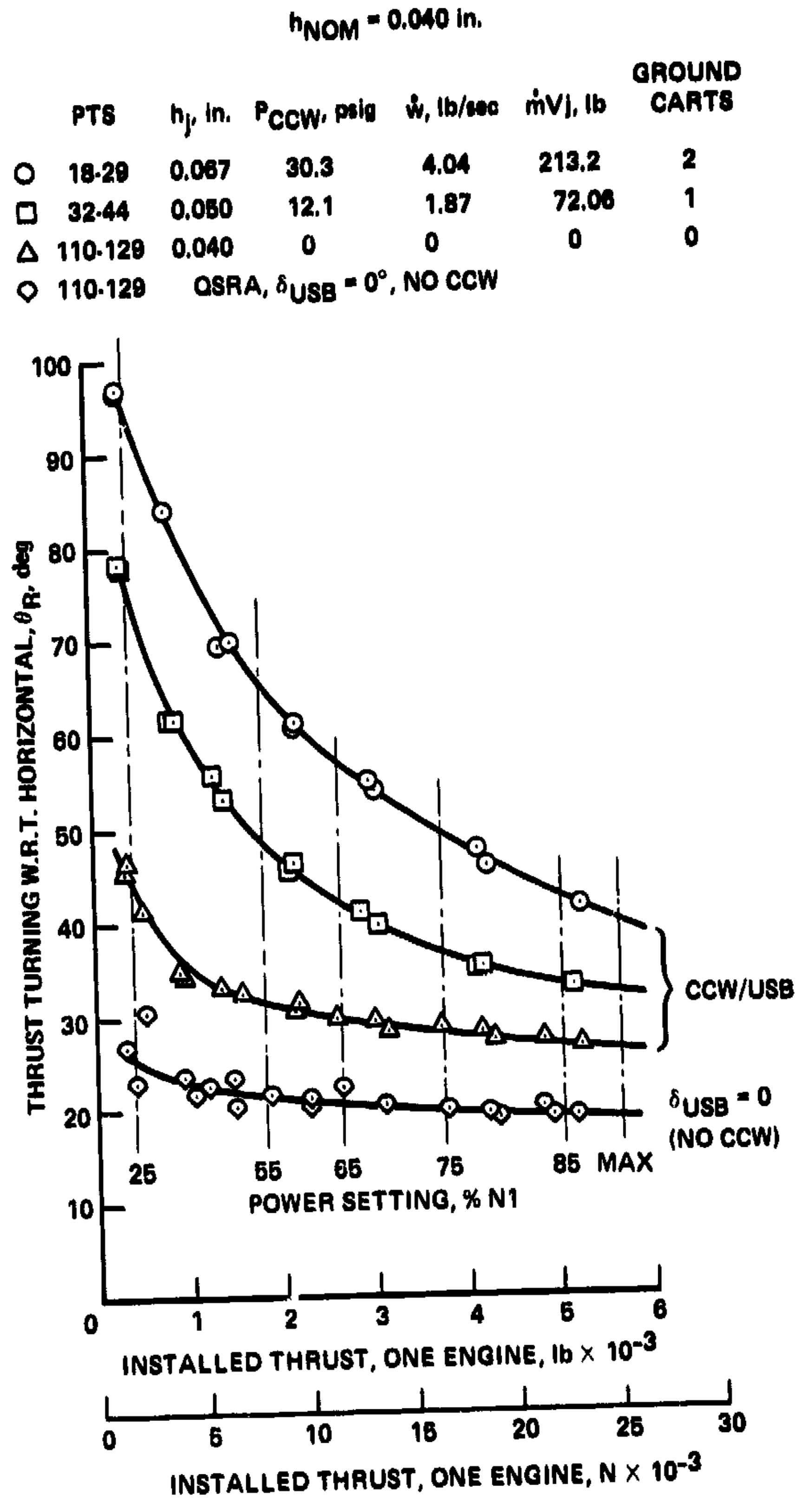

Figure 20. QSRA CCW/USB Static thrust turning vs. installed thrust.

h_{NOM} = 0.040 in.
SLOT SPAN = 74.5 in.

	PTS	h_j, in.	P_{CCW}, psig	$\dot{w}$, lb/sec	$\dot{m}V_j$, lb	GROUND CARTS
○	18-29	0.067	30.3	4.04	213.2	2
□	32-44	0.050	12.1	1.87	72.06	1
△	1-17	0.040	0	0	0	0
○	110-129	QSRA, δ_{USB} = 0°, NO CCW				
◊		QSRA, δ_{USB} = 66° (REF 8)				

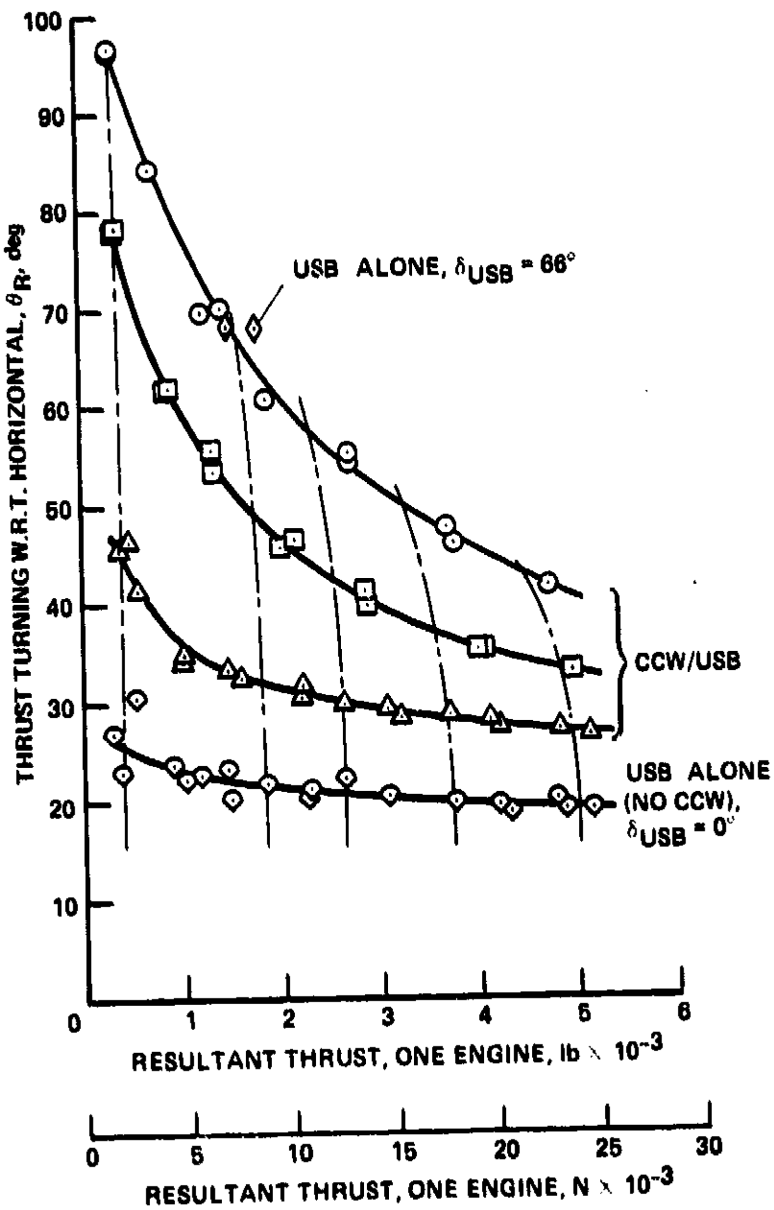

Figure 21. QSRA CCW/USB Static thrust turning vs. resultant thrust.

h_{NOM} = 0.020 in.
SLOT SPAN = 74.5 in.

	PTS	h_j, in.	P_{CCW}, psig	$\dot{w}$, lb/sec	$\dot{m}V_j$, lb	GROUND CARTS
○	47-59	0.050	33.5	3.32	174.7	2
□	63-75	0.037	18.7	1.72	76.4	1

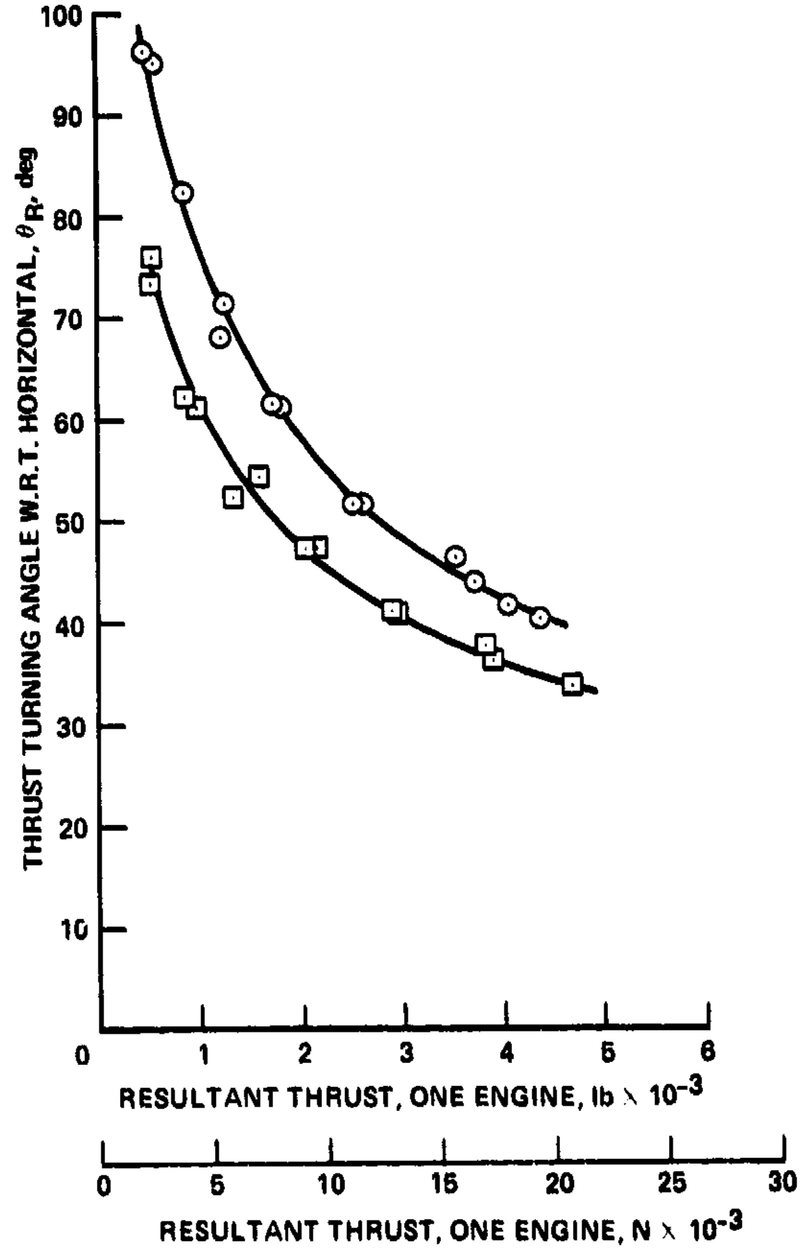

Figure 22. QSRA CCW/USB Static thrust turning vs. resultant thrust.

ORIGINAL PAGE IS
OF POOR QUALITY

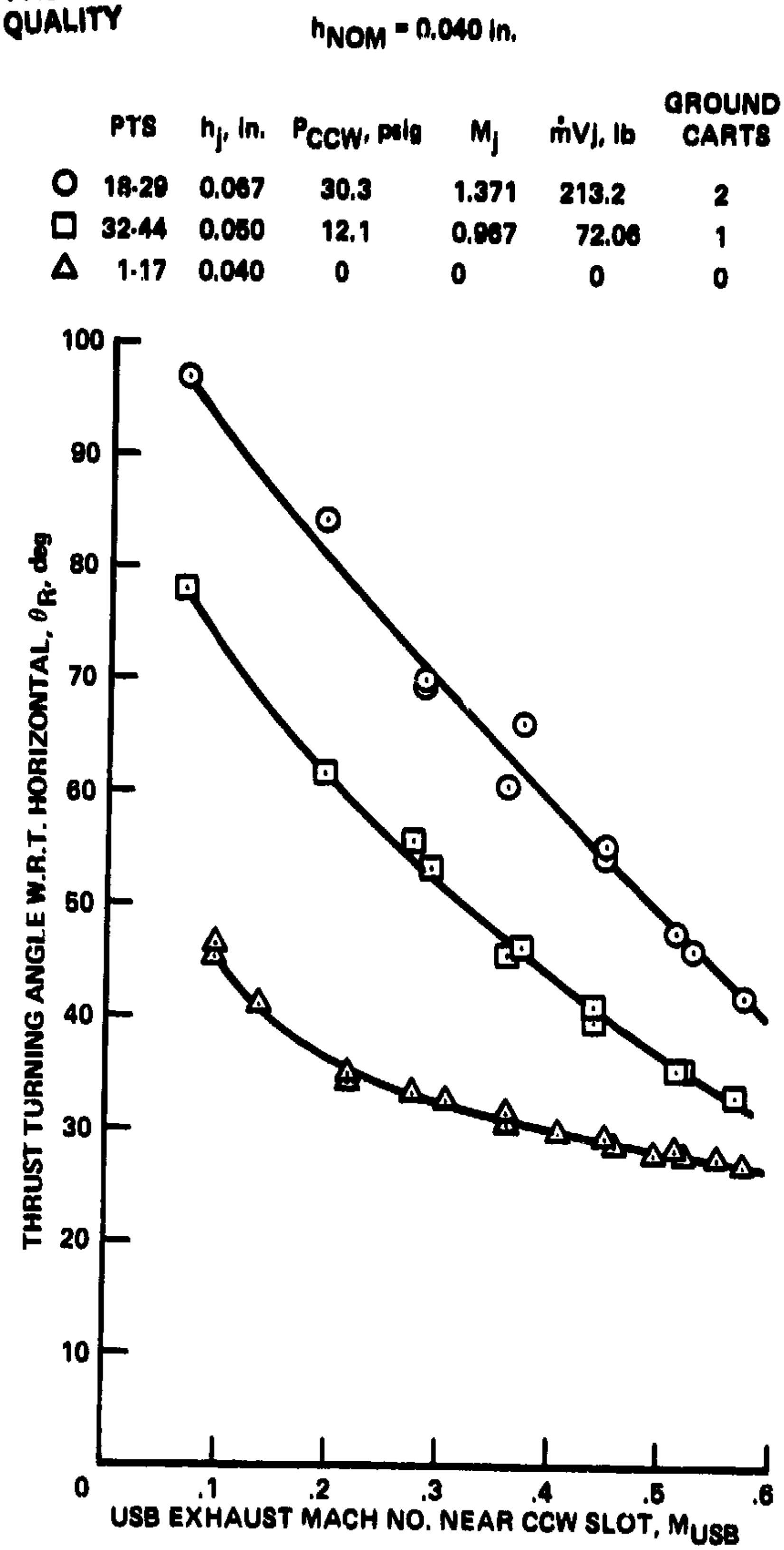

Figure 23. QSRA CCW/USB Static thrust turning vs. exhaust mach No.

h_{NOM} = 0.020 in.

	PTS	h_j, in.	P_{CCW}, psig	M_j	$\dot{m}V_j$, lb	GROUND CARTS
○	47-59	0.050	33.5	1.420	174.7	2
□	63-75	0.037	18.7	1.149	76.4	1

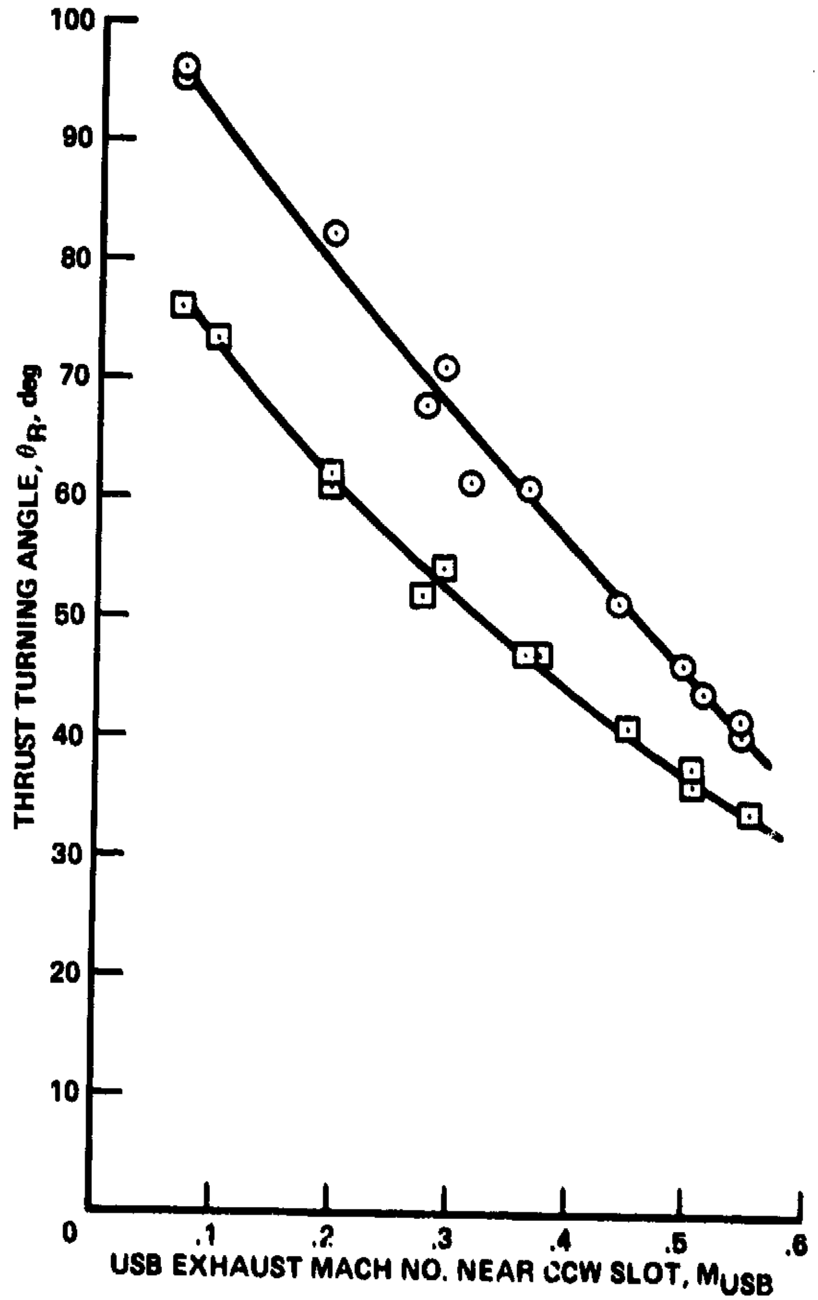

Figure 24. QSRA CCW/USB Static thrust turning vs. exhaust mach No.

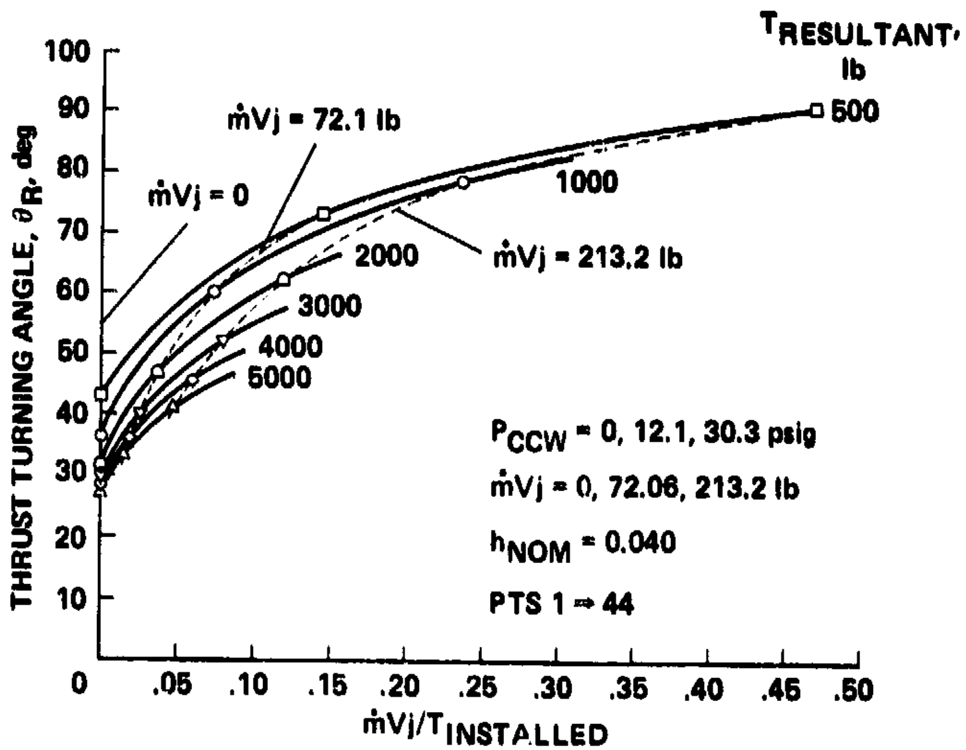

Figure 25. QSRA CCW/USB Static thrust turning vs. required CCW momentum.

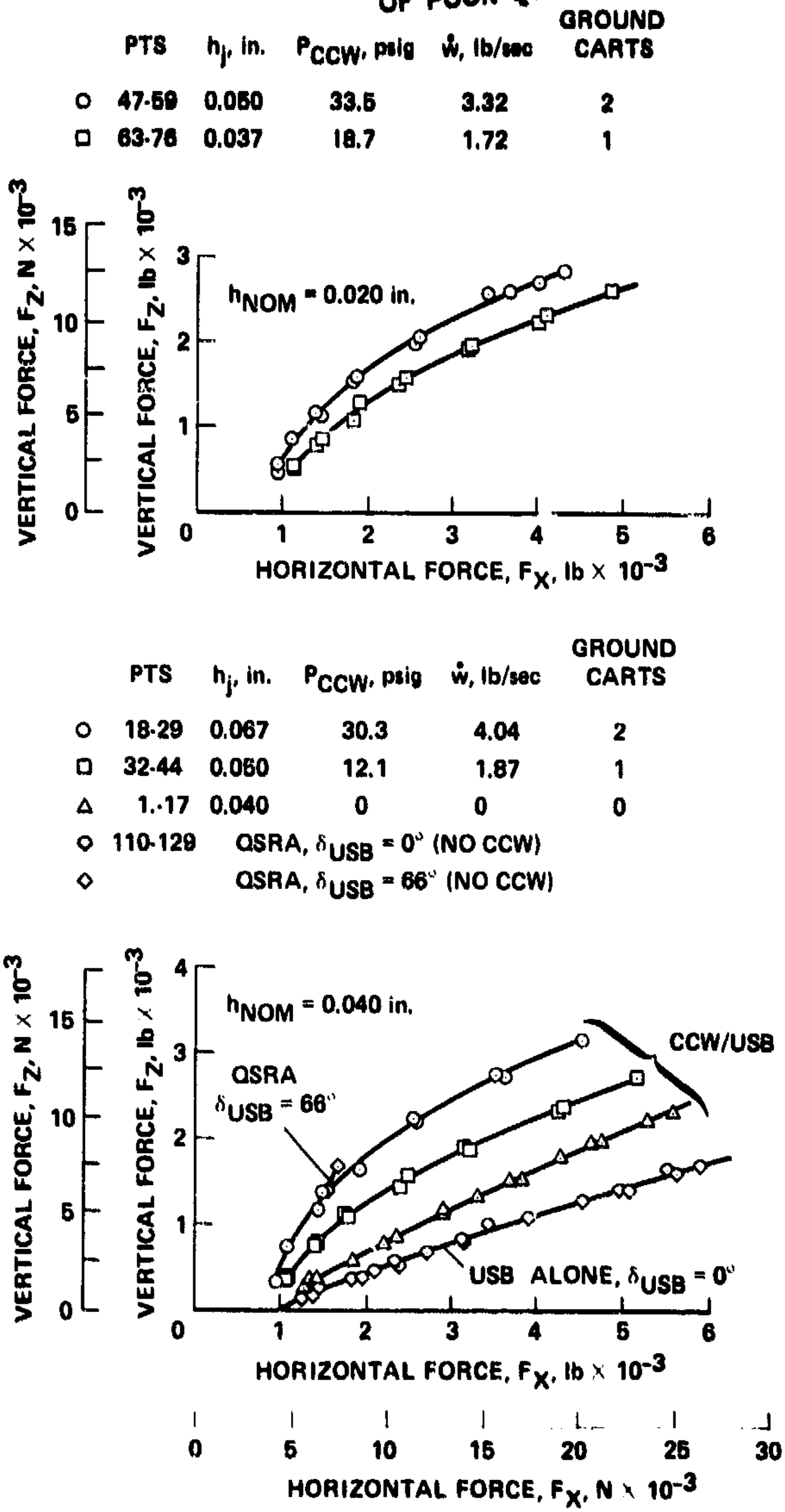

Figure 26. QSRA CCW/USB Static thrust components.

ORIGINAL PAGE
BLACK AND WHITE PHOTOGRAPH

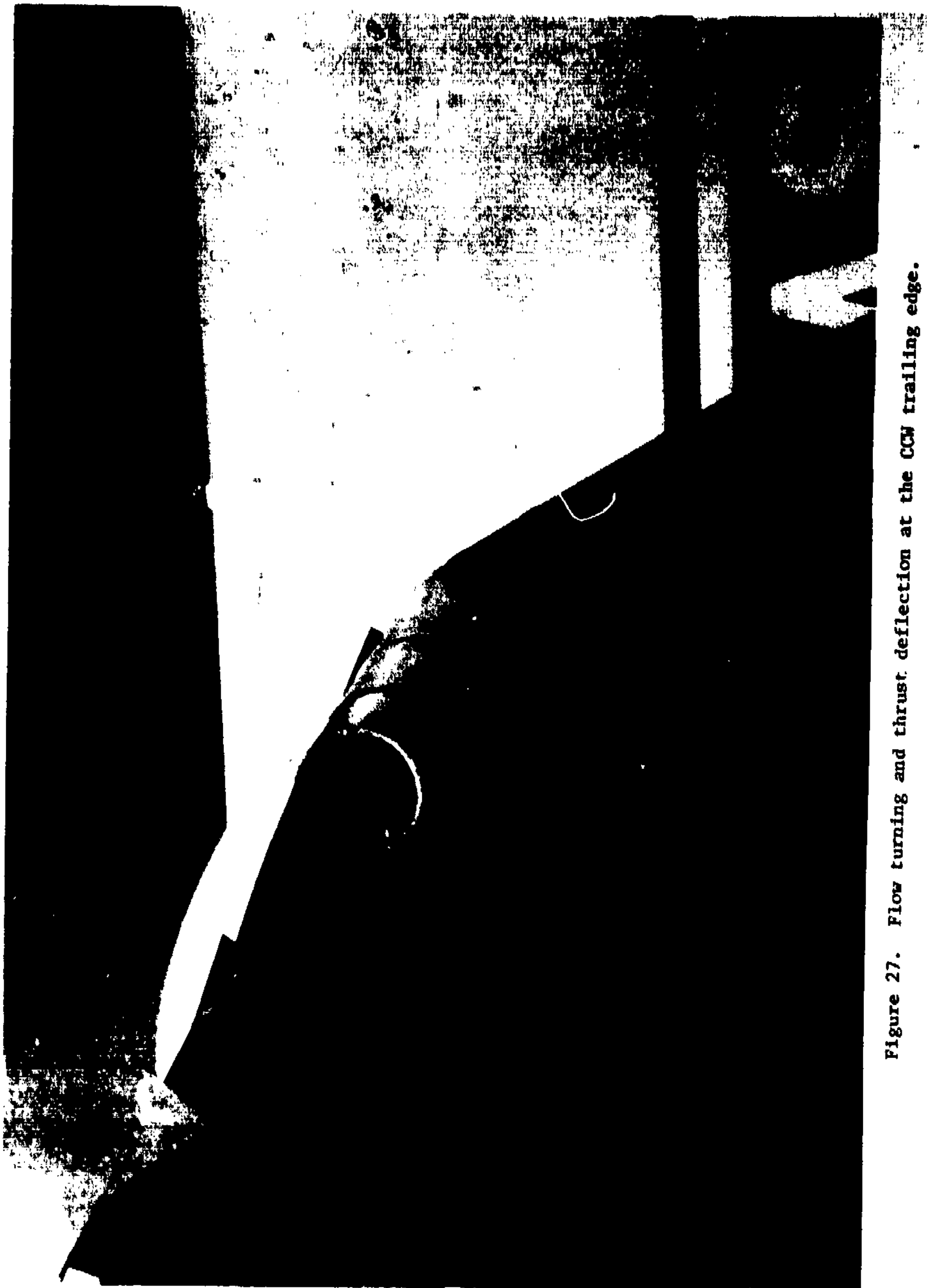

Figure 27. Flow turning and thrust deflection at the CCW trailing edge.

ORIGINAL PAGE IS
OF POOR QUALITY

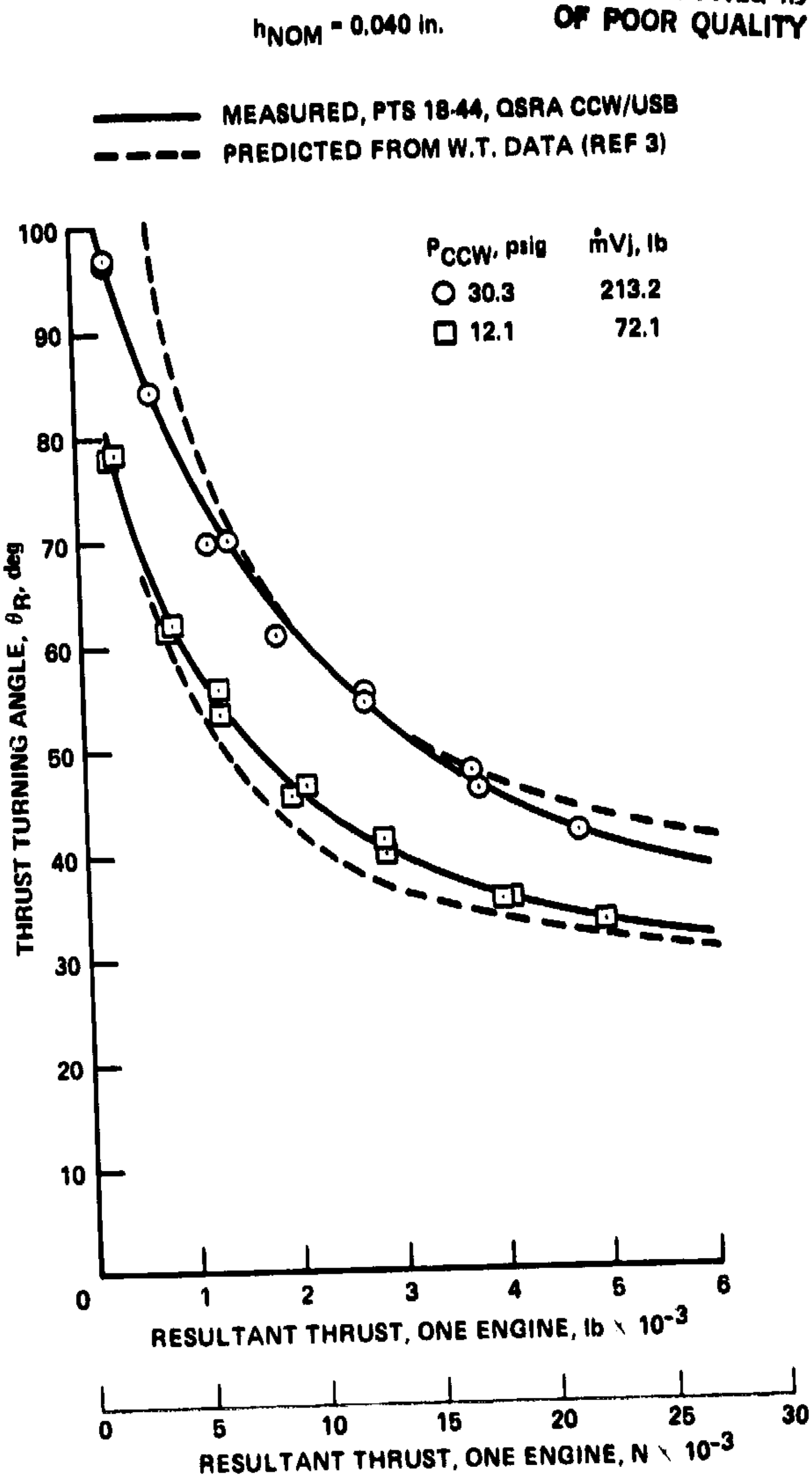

Figure 28. QSRA CCW/USB Static thrust turning, predicted vs. measured.

TABLE I
LISTING OF TEST POINTS

RUN	POINTS	POWER SETTING, % FAN SPEED	AIR CARTS	SLOT HEIGHT, m (in.)
1 BASELINE	1-17	23-87 (MAX.) 87-23	NONE	1.0E-03 (0.040)
2	18-31	23-87 (MAX.) 87-23	TWO	1.0E-03 (0.040) NOM. 1.7E-03 (0.067) ACTUAL
3	32-44	23-86 86-23	ONE	1.0E-03 (0.040) NOM. 1.27E-03 (0.050) ACTUAL
	45	0	ONE	1.27E-03 (0.050)
	46	0	TWO	1.7E-03 (0.067)
4	47-61	23-87 87-23	TWO	0.5E-03 (0.020) NOM. 1.27E-03 (0.050) ACTUAL
	62	23	NONE	0.5E-03 (0.020)
5	63-75	24-80 80-24	ONE	0.5E-03 (0.020) NOM. 9.4E-04 (0.037)
	76	29	ONE	7.1E-04 (0.028) ACTUAL
	77	0	TWO	8.9E-04 (0.035) ACTUAL
6 $\delta_{USB} = 0°$	110-129	23-87 87-23	NONE	